NADER C. DUTTA, RAN BACHRACH AND TAPAN MUKERJI

QUANTITATIVE ANALYSIS OF GEOPRESSURE FOR GEOSCIENTISTS AND ENGINEERS

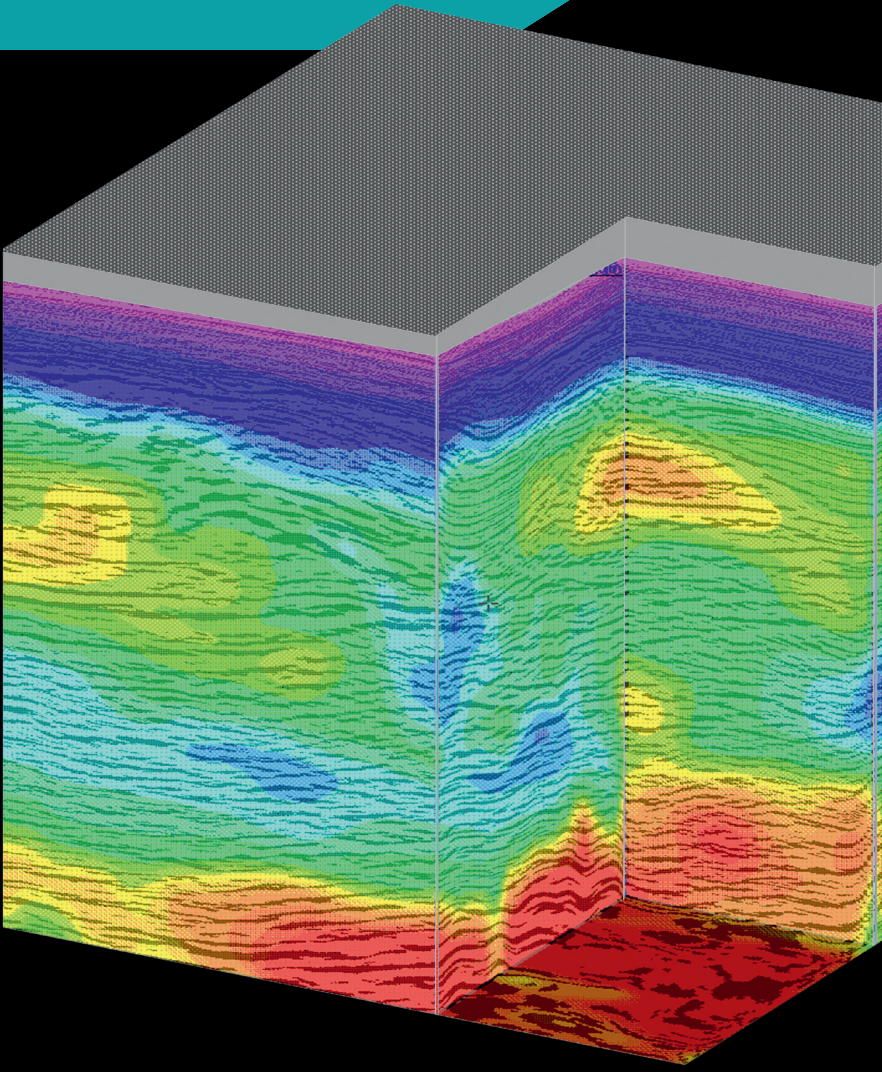

Quantitative Analysis of Geopressure for Geoscientists and Engineers

Geopressure, or pore pressure in subsurface rock formations impacts hydrocarbon resource estimation, drilling, and drilling safety in operations. This book provides a comprehensive overview of geopressure analysis, bringing together rock physics, seismic technology, quantitative basin modeling, and geomechanics. It provides a fundamental physical and geological basis for understanding geopressure by explaining the coupled mechanical and thermal processes. It also brings together state-of-the-art tools and technologies for analysis and detection of geopressure, along with the associated uncertainty. Prediction and detection of shallow geohazards and gas hydrates are also discussed, and field examples are used to illustrate how models can be practically applied. With supplementary Matlab codes and exercises available online, this is an ideal resource for students, researchers, and industry professionals in geoscience and petroleum engineering looking to understand and analyze subsurface formation pressure.

Nader C. Dutta is a recognized industry expert on geopressure and was the senior science advisor of Schlumberger prior to retiring in 2015. He is currently a visiting scholar at the Geological Sciences Department, Stanford University. He is the editor of SEG's book *Geopressure* (1987) and has been a member of United Nations Environmental Program (UNEP) and USA-DOE Gas Hydrate Assessment Committee.

Ran Bachrach is a scientific advisor for Schlumberger, supporting both research and operations and specializing in various geoscience topics, including high-resolution geophysics, rock physics and geomechanics, 3D/4D imaging of subsurface processes, seismic inversion, and seismic reservoir analysis.

Tapan Mukerji is a professor in the Department of Energy Resources Engineering and by courtesy in the Departments of Geophysics and Geological Sciences at Stanford University. He received the Society of Exploration Geophysicists' Karcher Award in 2000 and shared the 2014 ENI award for pioneering innovations in theoretical and practical rock physics for seismic reservoir characterization. He is also a coauthor of *The Rock Physics Handbook* (2020), *Value of Information in Earth Sciences* (2015), and *Quantitative Seismic Interpretation* (2005), Cambridge University Press.

Quantitative Analysis of Geopressure for Geoscientists and Engineers

NADER C. DUTTA
Stanford University

RAN BACHRACH
Schlumberger

TAPAN MUKERJI
Stanford University

CAMBRIDGE
UNIVERSITY PRESS

CAMBRIDGE
UNIVERSITY PRESS

University Printing House, Cambridge CB2 8BS, United Kingdom

One Liberty Plaza, 20th Floor, New York, NY 10006, USA

477 Williamstown Road, Port Melbourne, VIC 3207, Australia

314–321, 3rd Floor, Plot 3, Splendor Forum, Jasola District Centre, New Delhi – 110025, India

79 Anson Road, #06–04/06, Singapore 079906

Cambridge University Press is part of the University of Cambridge.

It furthers the University's mission by disseminating knowledge in the pursuit of education, learning, and research at the highest international levels of excellence.

www.cambridge.org
Information on this title: www.cambridge.org/9781107194113
DOI: 10.1017/9781108151726

First published 2021

Printed in the United Kingdom by TJ Books Limited, Padstow Cornwall

A catalogue record for this publication is available from the British Library.

Library of Congress Cataloging-in-Publication Data
Names: Dutta, Nader C., author. | Bachrach, Ran, 1967– author. | Mukerji, Tapan, 1965– author.
Title: Quantitative analysis of geopressure for geoscientists and engineers / Nader C. Dutta, formerly of Schlumberger, currently at Staford University, California, Ran Bachrach, Schlumberger, Tapan Mukerji, Stanford University, California.
Description: Cambridge, United Kingdom ; New York, NY, USA : Cambridge University Press, 2021. | Includes index.
Identifiers: LCCN 2020026301 | ISBN 9781107194113 (hardback) | ISBN 9781108151726 (ebook)
Subjects: LCSH: Reservoir oil pressure – Mathematical models. | Petroleum – Migration. | Fluid dynamics.
Classification: LCC TN871.18 .D88 2021 | DDC 553.2/82–dc23
LC record available at https://lccn.loc.gov/2020026301

ISBN 978-1-107-19411-3 Hardback

Additional resources for this publication at www.cambridge.org/geopressure.

Contents

Color plates can be found between pages 276 and 277.

Preface

How did we come to write this book? Our research suggested that the discipline of geopressure started based on fundamentals of geology (such as the pioneering works of Ruby and Hubbert and Dickinson during the middle of the twentieth century), with an excellent promise of delivery of applications to the hydrocarbon industry. As the quest for hydrocarbon exploration and exploitation required more and more integrated approaches, contributions from many diverse fields of sciences, such as geology, geophysics, petrophysics, applied physics, engineering, and applied mathematics, became the norm. However, quick-fix engineering approaches to tackle challenging problems at hand resulted in fragmented knowledge building and lack of emphasis on fundamentals. This was noted in an earlier publication (Dutta, 1987a, vii): "understanding of the geopressuring phenomenon is worth vigorous pursuit because that understanding calls for an integrated approach in unraveling its mysteries." We felt that the field of geopressure required another look – one that would culminate in a comprehensive discussion of the subject, including the industrial applications and an assessment of the road ahead. This is the goal of this book. Whether this goal is met awaits the judgment of our readers and peers.

During our professional careers, we have been fortunate enough to have witnessed some remarkable achievements in the field of geophysics, in particular, in the seismic subdiscipline. It has been propelled by high-speed computing with concomitant development of complex algorithms, such as tomography and full waveform inversion (FWI), by some brilliant geoscientists. This resulted in a step change in the subsurface seismic image quality. Therefore, some timely questions needed to be asked: Have we taken advantage of these opportunities in geopressure analysis that requires earth model building rather than velocity modeling? Are subsurface images at the right depths? Well, partly yes, but not consistently. Building *an earth model* requires a thorough understanding of the underlying basic physics to describe important subsurface phenomena, such as geopressure, among others. Just what would the effect on imaging be if we were to get this description on the right footing? This requires analysis of the geopressure phenomenon quantitatively, reliably, and making it accessible to all geoscientists and engineers so that integration with other viable model-building processes can take place. We hope the readers will appreciate the attempt undertaken in the book to address this issue.

The book has fourteen chapters that describe the geopressure phenomenon – fundamentals, models and mechanisms, and tools to predict and detect it – from borehole centric to seismic, taking care to explain the basic physics behind these tools, including limitations of their operating envelopes. We have come to understand better the physics of rocks through careful measurements, both in the laboratory and in the field, and through theoretical analysis. This has enabled us to develop and test subsurface models with more confidence and has helped us to extract rock properties from seismic attributes using sophisticated inversion technologies. The knowledge captured from this directly impacts our understanding of geopressure. Therefore, in this book, an attempt is made to put some of the known subsurface pore pressure models on firmer ground by providing a rock physics basis for some of these models. This allowed us to extend the traditional scale of geopressure prediction envelope from exploration – say, several hundred feet – to drilling around a borehole, at a few feet. To bridge this *scale* is to lay the foundation for a best-practice approach in geopressure and to enable us to extrapolate into what is yet to come. Nonetheless, it is a snapshot at the present and obviously colored by our own biases. We hope the future generation will build on it. A unique feature of this book deals with applications to illustrate how the geopressure models can be used not only for energy resources assessment but also for environmental issues. In this context, our experiences in dealing with prediction of subsurface geohazards, such as possible existence of shallow aquifer pressured sands in deepwater (aka shallow-water-flow sands), gas charged sands and gas hydrates, and various seabed hazardous features, will be beneficial not only to the energy resource developers and operators but also to regulatory agencies. The approach discussed in the book enables us to go beyond *color coding* a geohazard map – the current practice – to adding *qualifiers*, such as just how red is *red*, what is the extent of the *yellow*, and what is the comfort zone of the *green*? We address these geohazard issues quantitatively so that our sister community of drilling can benefit from closer interaction with geoscientists.

Several books are devoted to subsurface pressure; however, while they were classics during their times, their contents are now mostly outdated. Some other compilations consist of conference proceedings and reviews of papers dealing with special aspects of geopressure and do not include many recent and important developments. These may not be appropriate for students and researchers beginning their careers. This book aims to bridge the gap. To help the readers self-assess their understanding of various subjects addressed in the book, we have a companion website (see the Cambridge University Press site) with suggested exercises and Matlab codes.

By the time we finished the manuscript of the book, the world that we knew had changed. We are witnessing a pandemic incurred by COVID-19, resulting in many deaths and lockdowns in our homes. So the environment has changed drastically between the time we started the project some three years ago and the time when we finished it. However, the project provided some solace to us!

Now comes the most pleasant part of this preface – acknowledgments. There are so many that to mention all the names is practically impossible. Therefore, we sincerely apologize to those who contributed over the years but whose names are not mentioned. We benefited greatly from the scientific training received in the academy and the industry to the tune of more than 75 years of cumulative experience – through knowledge sharing with students, staff, and industry partners, often with hands-on experience and project management. This has broadened our curiosity, given us strength to march on, and empowered us with tools that resulted in this book. We are very grateful to those who gave us this opportunity. Special thanks are due to Jianchun Dai, Yangjun (Kevin) Liu, and Sherman Yang – all were dear colleagues of the senior author while he was employed at Schlumberger. Thanks, guys! On a personal note, Nader Dutta presented a good portion of this book in a training course at Stanford University in 2016. Feedback from students greatly impacted the presentation of the subject matter in the book. In particular, Anshuman Pradhan – soon to be Dr. Pradhan – deserves special thanks. He was the teaching assistant when the course in geopressure was taught at Stanford. Some of Anshuman's work is included in this book in Chapters 10 and 13. Thanks, Anshuman. Thanks are also due to Dr. Huy Le, who graduated recently with a PhD from Stanford and addressed a good part of his dissertation to link seismic imaging with pore pressure constraints using FWI. The methodology is partly based on some of the material that we discuss in Chapter 6. Thanks, Huy. The encouragement of his thesis advisor at Stanford, Professor Biondo Biondi, to share knowledge is greatly appreciated. Dr. Allegra Hosford-Scheirer at Stanford provided a very constructive environment to carry on integrating basin modeling to imaging through pore pressure. Her enthusiasm and energy are legendary and inspirational to all. Thanks, Allegra! Gary Mavko provided great encouragement and practical advice – finish the book first! Thanks, Gary! Here it is! We are grateful to the members of the following affiliate groups at Stanford University for sponsoring our work over the years and for funding Nader Dutta's stay at Stanford: Stanford Rock and Borehole Geophysics (SRB), Stanford Exploration Project (SEP), Basin and Petroleum System Modeling (BPSM), and the Stanford Center for Earth Resources Forecasting (SCERF). We acknowledge additional funding from Prof. Steve Graham, Dean of the Stanford School of Earth, Energy, and Environmental Sciences. We acknowledge Schlumberger for donations of software and data used in the work of Anshuman Pradhan and Huy Le, described in this book. A special thanks to Susan Francis and Sarah Lambert of Cambridge University Press for guiding us through this project – a long and arduous journey that finished with exhilaration. Thanks! Last, but not the least, Nader Dutta is grateful to his loving spouse, Chizuko, for providing gentle and timely criticism of the manuscript and sharing his joys as well as his frustrations – there were many!

Good reading, folks! Have fun!

1 Basic Pressure Concepts and Definitions

1.1 Introduction

Geopressure is the pressure beneath the surface of the earth. It is also known as the formation pressure. This could be lower than, equal to, or higher than the normal or hydrostatic pressure for a given depth. Hydrostatic or normal pressure is the force exerted per unit area by a column of freshwater from the earth's surface (e.g., sea level) to a given depth. Geopressures lower than the hydrostatic pressures are known as underpressures or subpressures, and they occur in areas where fluids have been drained, such as a depleted hydrocarbon reservoir. Geopressures higher than hydrostatic pressures are known as overpressured, and they occur worldwide in formations where fluids are trapped within sediments due to many geologic conditions and support the overlying load. Overpressured formations are also known as formations with abnormally high pore pressure. The lithostatic (or overburden) pressure at a given depth is due to the *combined* weight of the overlying rock and fluids. The fracture pressure is the pressure that causes the formation rock to crack. Figure 1.1 shows these concepts in graphical terms.

If the overlying fluid is composed of hydrocarbon as well as water (brine), the pressure versus depth plot will look like that shown in Figure 1.2.

The slope changes in the plot are due to density differences between brine, oil, and gas. The overpressure phenomenon is well known throughout the world. Among other things, the magnitude and distribution of overpressure in sedimentary basins have been known to critically impact the evolution of hydrocarbon provinces, control the migration of fluids within a basin, and affect the processes that are used to mine the subsurface resources, such as oil and gas. The most discussed and well-known cause of overpressure is the rapid burial of low-permeability water-filled sediments (e.g., clay) at a rate that does not allow the fluid to escape fast enough to maintain hydrostatic equilibrium upon further burial. Thus, further burial causes geopressure to rise even more. This is known as compaction disequilibrium. This is the leading cause of overpressure in most of the Tertiary clastic basins of the world, such as the Gulf of Mexico. This and many other mechanisms of overpressure are discussed in detail in Chapter 3.

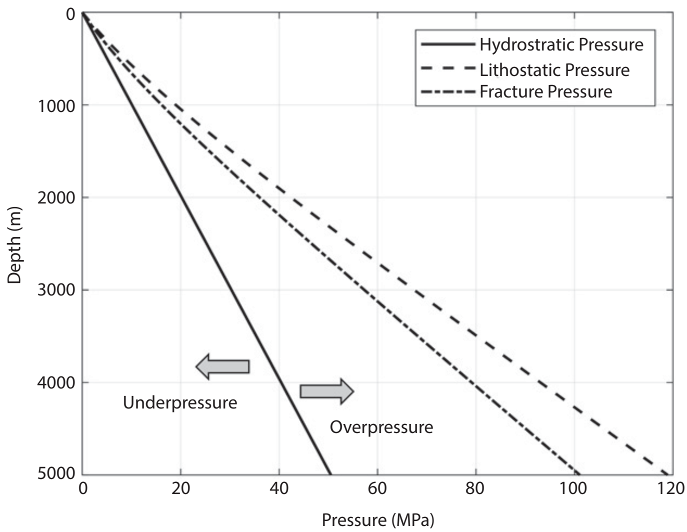

Figure 1.1 Pressure versus depth plot showing geopressure regimes.

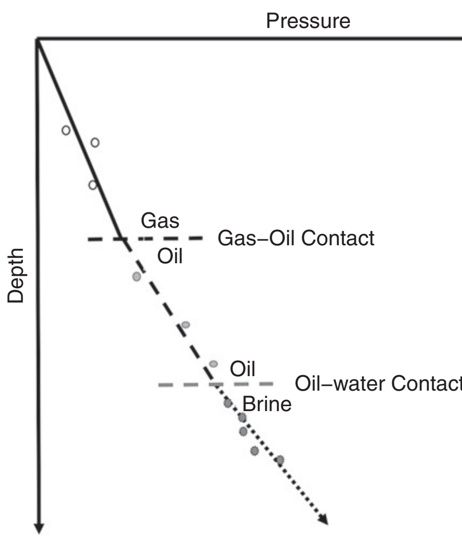

Figure 1.2 Pressure versus depth plot showing buoyancy effect due to hydrocarbons.

1.2 Basic Concepts

1.2.1 Units and Dimensions

Before we proceed, a word on units and dimensions is in order. All quantities in physics must either be dimensionless or have dimensions. All units can be expressed in terms of mass [M], length [L], and time [T]. In equations, the units must be consistent; there is no need for conversion factors. However, care is needed for quantities, such as pressure. It is force per unit area. The dimension of force is [$ML^{-1}T^{-2}$]; but if the unit of length is feet and the unit of pressure is pounds per square inch, or psi (as is commonly used in the US drilling community), a conversion factor is required, since these are inconsistent mixed units. In SI units, such conversion factors are not needed because all the units are consistent. The lack of inconsistency of units using the American system is known to have created a massive headache between the two drilling communities – those who use the SI units (some communities in Europe, for example) and those who do not use SI units. We shall discuss this further in this chapter in the context of pore pressure measurements.

As mentioned, pore pressure has the dimension of force per unit area. In the SI system, the unit of pressure is pascal (Pa), and in the British system, the unit is pounds per square inch (psi). We note that 1 Pa = 1.4504×10^{-4} psi. This is a rather small unit, and for most practical applications, it is customary to use either kilopascal (KPa) or megapascal (MPa). Drillers, engineers, and well loggers still use the British system, while the academicians prefer the SI system. Therefore, a fluency in both type of units is a must. We will be using the mixed system throughout the book. However, whenever possible, we will provide the SI or British system equivalents.

1.2.2 Hydrostatic Pressure

Sedimentary rocks in formations are composed of solid material and fluids in the porous network. Hydrostatic or normal pressure, P_h, is the pressure caused by the weight of a column of fluid and is given by

$$P_h = \int_0^z \rho_f(z) g dz + Pair \approx \rho_f g z + P_{air} \tag{1.1}$$

where z is the column height of the fluid, ρ_f is the density of the fluid, g is the acceleration due to gravity, and P_{air} denotes the pressure due to the atmosphere. The size and shape of the fluid column have no effect on hydrostatic pressure. The approximation on the right-hand side of equation (1.1) assumes that ρ_f is constant and z is the depth below sea level or the land surface. Hydrostatic pore pressure increases with depth; the gradient at a given depth is dictated by the fluid density at that depth. This is because the water or brine density is not constant. Water tends to expand with rising temperature but contracts with rising pressure. As we shall see later, between the two processes in the subsurface (i.e., increase in temperature and pressure), thermal expansion with increasing depth is greater than the mechanical compression. There are other factors that affect the water density, such as dissolved salt – the solubility of salt also increases with depth. Subsurface brines are more saline than the ocean water. This increase in total dissolved salt increases the density of water. The net effect is that the water (brine) density is a complex function of temperature, pressure, and total dissolved solids. If a subsurface formation is in the hydrostatic condition, it implies that there is an interconnected and open pore system from the earth's surface to the depth of measurement. To summarize, the fluid density depends on various factors, such as fluid type (oil, water, or gas), concentration of dissolved solids (i.e., salts and other minerals), and temperature and pressure of the fluid and gases dissolved in the fluid column. In Appendix A we provide some practical empirical relationships for physical properties of brine, gas, and oil needed for quantitative analysis of geopressure.

We strongly recommend that those who wish to pursue quantitative evaluation of geopressure use those equations for density and velocity of brine, gas, and oil ("dead" and "live") in a computer code. This will enable them to evaluate the true hydrostatic pressure as well as the pressure due to gas and oil columns of various heights. Here "dead" oil designates oil without any dissolved gas, whereas "live" oil means it contains dissolved gas.

What would a pressure versus depth plot such as the one in Figure 1.1 look like for a reservoir rock containing gas, oil, and water? An example is given in Figure 1.2 for the case of a reservoir filled with gas, oil, and water (brine). The slope changes are due to the density contrast between different kinds of fluids (gas, oil, brine), as discussed earlier. This kind of plot is very useful for determining the height of a hydrocarbon column in a reservoir. The discrete data points show actual measurements of pore pressure in a reservoir. Typically, not many measurements are carried out, as measurements are expensive in a real petroleum well; petroleum engineers make these discrete measurements and then look for slope changes to determine gas–oil and oil–water contacts, which yield the hydrocarbon column height. Eventually, seismic data are used along with geologic structure maps of a prospect to map these contacts in 3D. Volumetric calculations resulting from these measurements, along with uncertainty estimates, are used to determine the ultimate value of the asset.

1.2.3 Head

We introduce some terminology commonly used in fluid dynamics and relevant to geopressure. In the subsurface, fluids always move, although the speed at which they move is small in the human timescale. It is not so in the geologic timescale. The definitions that we gave in Section 1.2.2 are for fluids in the static condition. In fluid mechanics literature, the word *head* is commonly used. *Head* refers to a vertical dimension and has the dimension of length [L]. There are various types of heads.

A *pressure head* (also termed as *static pressure head* or *static head*) is the vertical elevation of the free surface of water above the point of interest. It is given by

$$\psi = P/\gamma = P/\rho g \tag{1.2}$$

where

ψ is the pressure head (length, typically in units of m)
P is the fluid pressure (force per unit area, typically in units of Pa)
γ is the specific weight (force per unit volume, typically in units of Newton/m^3)
ρ is the density of the fluid (mass per unit volume, typically in kg/m^3)

The term *hydraulic head* or *piezometric head* is used to specify a specific measurement of liquid pressure above a *datum*. It is composed of three terms: velocity head (h_v), elevation head ($z_{\text{elevation}}$), and pressure head (ψ). The following is referred to as the *head equation*:

$$C = h_v + z_{\text{elevation}} + \psi \tag{1.3}$$

Here C is a constant for the system (referred to as the *total head*) that appears in the context of the Bernoulli equation for incompressible fluids in hydrodynamics, which states that an increase in fluid speed occurs simultaneously with a decrease in pressure (Streeter, 1966). The *velocity head* (also referred to as *kinetic head*) is the head due to the energy of movement of the water. (In subsurface flow through porous rocks, this is negligible.) The *elevation head* is the elevation of the point of interest above a datum, usually sea level or the land surface.

1.3 Pore Pressure Gradient

A gradient is the first derivative of a physical quantity. The pressure gradient, dp/dz, is the *true* gradient of pore pressure, p, versus depth at a given point z. It shows change of pore pressure in a small scale. It is the rate at which pressure varies along a uniform column of fluid due to the fluid's own weight. Thus, a change in gradient implies a change in fluid density. Local gradients are most useful when working with the absolute pressure. However, the drilling community uses a term called *pore pressure gradient* to denote the density of fluid. It is the ratio of the pore pressure (p at a depth z) to the depth z. This is usually expressed in pounds per square inch per foot (abbreviated by psi/ft) in the British system of units and MPa/m in the SI system. It is clear that this gradient is *datum* dependent. Furthermore, pore pressure gradient is *not the true gradient* of p as a geoscientist or an engineer would define. It is simply pressure/depth. The conversion between fluid density and fluid pressure gradient is

$$1 \text{ psi/ft} = 2.31 \text{ g/cm}^3$$
$$\text{Thus } 1 \text{ psi/ft} = 2.31 \text{ g/cm}^3 = 0.0225 \text{ MPa/m} = 22.5 \text{ kPa/m} \tag{1.4}$$

Thus, the fluid density, can be defined as

$$\text{fluid density (g/cm}^3) = 0.433 \text{ (psi/ft)} \tag{1.5}$$

The drilling community uses a term called *equivalent mud weight* (EMW) to denote the density of fluid (mud) required to drill a well. It is expressed in pounds per gallon, abbreviated as ppg. A conversion factor for equivalent mud weights is

$$1 \text{ lb/gal or } 1 \text{ ppg} = 0.0519 \text{ psi/ft} \tag{1.6}$$

Weight in itself is not a gradient. If we relate weight to a volume, however, we have density, and density does convert to a gradient. When we refer to mud weights as 10 pounds, we mean the mud *density* is 10.0 lb/gal or ppg. This is a density. (In this nomenclature, pure water density would be 8.344 ppg.) Fertl (1976) suggested the following relation for hydrostatic pressure in psi, as is commonly used in drilling operations:

$$P_h = CM_w z \tag{1.7}$$

where z is the vertical height of fluid column in feet, M_w is fluid density for mud weight expressed in lb/gal (or ppg) or pounds per cubic feet (lb/ft^3), and C is a conversion constant equal to 0.0519 if M_w is expressed in pounds per US gallon and 0.00695 if M_w is expressed in lb/ft^3. The conversion factor 0.0519 (inverse of 19.250) is derived from dimensional analysis as follows:

$$\frac{1\text{psi}}{\text{ft}} = \frac{1\text{ft}}{12\text{in}} \times \frac{1\text{lb/in}^2}{1\text{psi}} \times \frac{231\text{in}^3}{1\text{USgal}} = 19.250\text{lb/gal} \tag{1.8}$$

It would be more accurate to divide a value in lb/gal by 19.25 than to multiply that value by 0.052. The magnitude of the error caused by multiplying by 0.052 is approximately 0.1 percent. Let us take an example: for a column of freshwater of 8.33 pounds per gallon (lb/US gal or ppg) standing still hydrostatically in a 21,000 ft vertically cased wellbore from top to bottom (vertical hole), the pressure gradient would be

$$\text{Pressure gradient} = 8.33/19.25 = 0.43273 \text{ psi/ft} \tag{1.9}$$

and the hydrostatic *bottom hole pressure* (BHP) is then BHP = true vertical depth × pressure gradient = 21,000 (ft) × 0.43273 (psi/ft) = 9087 psi. However, the formation fluid pressure (pore pressure) is usually much greater than the pressure due to a column of freshwater, and it can be as much as 19 or 20 ppg. For an onshore vertical wellbore with an exposed open hole interval at 21,000 ft with a pore pressure gradient of 19 ppg (or 19 × 0.0519 (psi/ft)), the BHP would be BHP = pressure gradient × true vertical depth = 19.0 × 0.0519 (psi/ft) × 21,000 (ft) = 20,708 psi. (It would be 20,727 psi if we replace 0.0519 by 1/19.25.) The calculation of a bottom hole pressure and the pressure induced by a static column of fluid (drilling mud) are the most important and basic calculations in the petroleum industry. In summary, pore pressure gradient is a *dimensional* term used by drilling engineers and mud engineers during the design of drilling programs for drilling (constructing) of oil and gas wells into the earth. In Table 1.1 we give some useful conversion factors.

In the Gulf Coast of the United States, a fluid pressure gradient of 0.465 psi/ft is considered to be normal or hydrostatic; it corresponds to a salt concentration of 80,000 ppm and a temperature of 77°F. However, the hydrostatic pressure gradient is variable depending upon the temperature, pressure, and salinity, as noted earlier. An increase in salt concentration at a given temperature and pressure would increase the hydrostatic gradient. Dissolved gas in water, for example, methane, also affects the density of water – it lowers the density – and hence the hydrostatic gradient will be lower. We

Table 1.1 Units and conversions

Psi	= 0.070307 kg. force/cm^2
Atm	= 1.033 kg force/ cm^2
Atm	= 14.6959 psi
Psi	= 0.006895 MPa
Psi/ft	= 2.31g/cm3
	= 1 4 4 lb / ft^3
	= 19.25 lb/gallons or ppg
1 Pa = 1N/m^2 = 1.4504 x 10^{-4} psi	
1 Mpa = 10^6 Pa = 145.0378 psi	
1 Mpa = 10 bars	
1 N = 1 kg. m/s^2	
1 kbar = 100 MPa	
1 psi / ft. = 2.31 g/cm^3	
$\approx 0.0225 MPa/m = 22.5 kPa/m$	

note that the solubility of methane in water is a function of salt concentration at a given temperature and pressure – it increases with increasing salt concentration. Thus, dissolved gases would cause the hydrostatic gradient to be lower. In the vicinity of salt domes, salt concentration could be markedly higher, leading to a higher hydrostatic gradient. In Table 1.2 we show typical values for density and pressure gradients for oil, brine, and some drilling fluids. In Table 1.3 we show typical hydrostatic pressure gradients for several areas of active drilling.

It is clear from these discussions that hydrostatic (or normal) pressure for a static water column of height z is equivalent to a water-saturated porous medium such as clean sandstone of the same height with the assumption that the sandstone consists of interconnected pores. Formation pressure (or geopressure) that *differs* from hydrostatic pressure is defined as *abnormal pressure.* Formation pressure (or geopressure) *exceeding* hydrostatic pressure is defined as *overpressure*, whereas formation pressure *lower* than hydrostatic is defined as *subpressure*. Therefore, we emphasize that before embarking on any computation involving determination of subsurface pore pressure, we must establish a proper baseline – deciding on the "accurate" hydrostatic pressure gradient with as much accuracy as possible.

1.4 Overburden Stress

The *overburden* or *lithostatic stress*, S, at any depth, z, is the stress that results from the *combined* vertical weight of the rock matrix and the fluids in the pore space overlying the formation of interest as well as the weight of the static water column, if in an offshore environment, and the atmospheric air pressure. This can be expressed as

$$S = P_{\text{air}} + g\int_{0}^{z_w} \rho_{sw}(z)dz + g\int_{z_w}^{z} \rho_b(z)dz \tag{1.10}$$

Table 1.2 Fluid densities and corresponding pressure gradients

Fluid	Total solids (ppm)	Density (g/ml)	Fluid pressure gradient (psi/ft)	(kPa/m)
Freshwater	0	1.0	0.433	9.8
Brine	28,000	1.02	0.441	10.0
	55,000	1.04	0.450	10.2
	84,000	1.06	0.459	10.4
	113,000	1.08	0.467	10.6
	144,000	1.10	0.476	10.8
	176,000	1.12	0.485	11.0
	210,000	1.14	0.493	11.2
Oil	API° (60°F)			
	70.6	0.70	0.303	6.90
	45.40	0.80	0.346	7.80
	25.70	0.90	0.390	8.80
	10.00	1.00	0.433	9.80
Drilling mud	lb/gal or ppg			
	8.35	1.00	0.433	9.80
	10.02	1.20	0.520	11.8
	11.69	1.40	0.607	13.70
	13.36	1.60	0.693	15.70
	15.03	1.80	0.780	17.70
	16.70	2.00	0.867	19.60
	18.37	2.20	0.953	21.60
	20.04	2.40	1.040	23.50
	21.71	2.60	1.126	25.50
	23.38	2.80	1.213	27.50
	25.05	3.00	1.300	29.40

Note: Pressure gradients are related to the specific gravity (γ) rather than the density (ρ), where $\gamma = \rho g$, $g = 9.81\ \mathrm{m/s^2}$.
Source: Modified after Gretener (1981)

Table 1.3 Normal pore pressure gradients for several areas

Area	Pressure gradient (psi/ft)	Pressure gradient (g/cc)
West Texas	0.433	1.000
Gulf of Mexico (coastline)	0.465	1.074
North Sea	0.452	1.044
Malaysia	0.442	1.021
Mackenzie Delta	0.442	1.021
West Africa	0.442	1.021
Anadarko Basin	0.433	1.000
Rocky Mountains	0.436	1.007
California	0.436	1.014

where P_{air} is the pressure due to the atmospheric air column (typically 14.5 psi or 1 bar), ρ_b is the bulk density, ρ_{sw} is the sea water density (both depend on depth), z_w is depth to the ocean bottom, and g is the acceleration due to gravity. The bulk density of a fluid-saturated rock is given by

$$\rho_b = (1 - \phi)\rho_r + \phi \rho_f \tag{1.11}$$

where ϕ is the fractional porosity (the void space in the rock), ρ_f is the pore fluid density, and ρ_r is the density of the matrix (grain density). It should be noted that the overburden stress computation in the context of drilling wells should always account for the air gap or the atmospheric pressure. Although this is small, it could be significant while dealing with overburden stress in shallow formations, such as pressured aquifer sands or methane hydrates, as discussed later. Overburden stress is *depth dependent* and increases with depth in a nonlinear fashion. In some of the older literature on geopressure, a default value of 1.0 psi/ft for overburden stress gradient (overburden stress divided by depth) has been recommended for the "average" Tertiary deposits off the Texas–Louisiana coast. This corresponds to a force exerted by a formation with an *average* bulk density of 2.31 g/cm^3. However, this is not true in reality, where we always deal with rocks of variable bulk densities. At shallower depths, the overburden gradient would be less than 1.0 psi/ft, while at deeper depths, it could be larger than 1.0 psi/ft. In Figure 1.3 we show typical overburden gradients from selected basins.

1.5 Effective Vertical Stress and Terzaghi's Law

When a rock is subjected to an external stress, it is opposed by the fluid pressure of pores in the rock. This is due to Newton's law of classical mechanics. More explicitly, if P is the formation or pore fluid pressure at a depth where the vertical component of the total stress (namely, the vertical overburden stress) on it is S, then the vertical effective stress σ is defined as (see Figure 1.4)

$$\sigma = S - P \tag{1.12}$$

This is known as the Terzaghi's principle or law (Terzaghi, 1923). This principle was invoked to describe the consolidation of soil in the context of geotechnical engineering (soil consolidation) (see Chapter 2). Compaction is due to the vertical effective stress – it is the stress that is transmitted through the solid framework. This (vertical effective stress) is a very important parameter to describe geopressure phenomenon quantitatively, especially when geophysical methods such as seismic or sonic logs are used to quantify geopressure. A relationship between velocity and overpressure is intuitively expected, since acoustic velocity and vertical effective stress are related closely. This will be discussed in Chapter 3. We note that

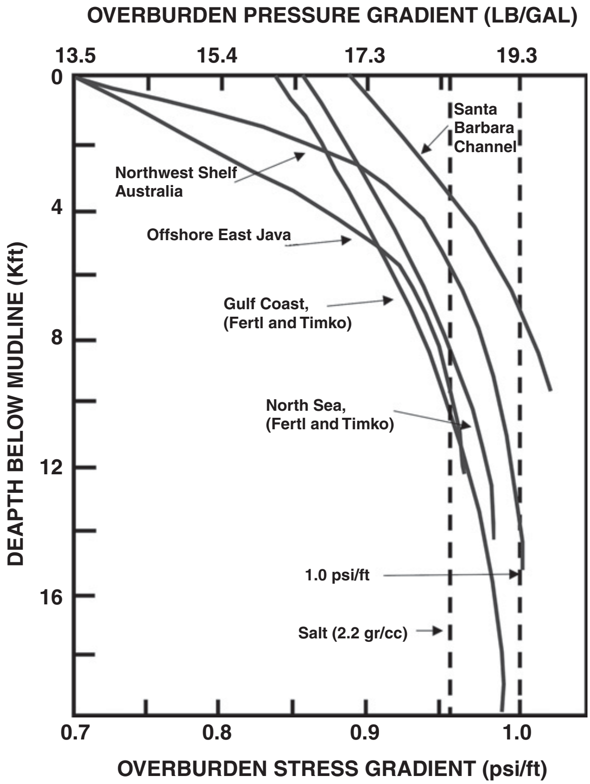

Figure 1.3 Typical overburden stress gradients versus depth in psi/ft and ppg. Modified after Dutta (1987a).

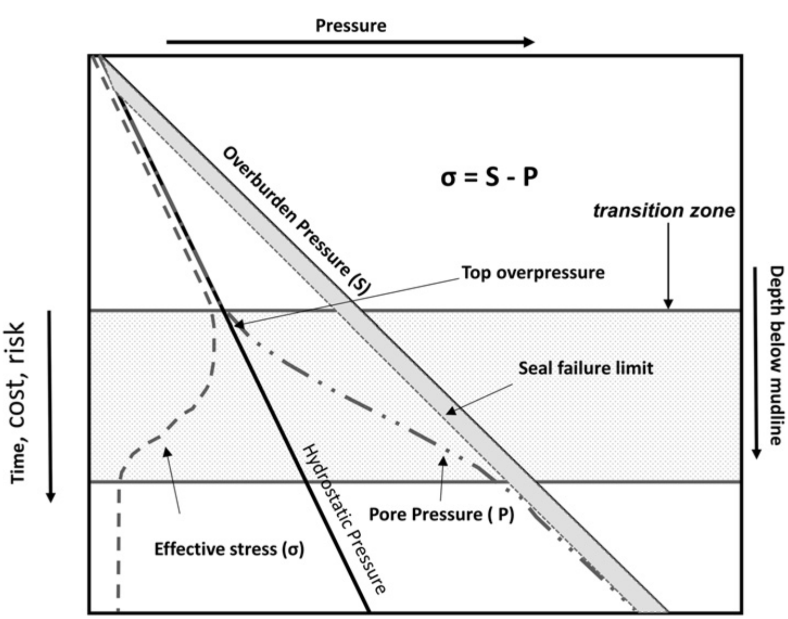

Figure 1.4 Subsurface pressure environment and some commonly used definitions. Modified after Dutta (1987a).

Terzaghi's Law is only an approximation because the vertical component of the total stress S does not remain constant in a sedimentary basin that is actively developing and accumulating sediment, nor does it remain strictly constant during compaction of sedimentary rocks (see Chapter 2). It has several other assumptions as well: The soil is isotropic and homogenous; the solid particles and fluids are incompressible; the fluid flow occurs in one dimension only (vertical direction); the strains in the soil are very small (linearized strain model); Darcy's law for fluid flow is valid for all pressures (linearized fluid flow model); the permeability remains constant throughout the process; and lastly, compaction process is independent of time. While some of the assumptions are reasonable and borne out by experiments, the remainder of the assumptions such as the linearity of strain, one-directional flow model as well as the time-independence of the compaction process (relationship between porosity and vertical effective stress) may be questioned.

Subsequent literature such as Hornby et al. (1994, and references therein) as well as Sarker and Batzle (2008, and references therein) suggested using the Biot model for the effective stress as given below, instead of Terzaghi's Law (see Chapter 2):

$$\sigma = S - \alpha P \tag{1.13}$$

where α is termed as Biot's consolidation coefficient and its value lies between 0 and 1. Further, it was mentioned that this coefficient could depend on the lithology also. Sarker and Batzle (2008) and Hornby et al. (1994) suggested that α is close or equal to unity for near-surface sediments such as soil and clay – the subject of measurements by Terzaghi (1923) but for consolidated rocks, it could be less than unity and its value is ~ 0.90 to 0.93 as determined by laboratory measurements using ultrasonic waves (Hornby et al., 1994). Suffice it to say at this point that the uncertainty regarding α is related to three major factors: (1) what are the "assumed" physical processes by which unconsolidated sediments morph into rocks under gravitational loading and many chemical effects? (2) How are the measurements conducted, namely, under static or dynamic conditions? and (3) what kind of rock types are considered in the measurements? It must be noted that there is no direct way to measure α; it is derived indirectly from measurements of physical quantities which are related to the effective stress such as pore pressure and velocity. We note that Biot's consolidation coefficient plays an important role in building geomechanical models (see Chapter 12). *In our discussions in this book we shall continue to use $\alpha = 1$ and the original version of the Terzaghi's Law as given in* equation (1.12) *unless otherwise stated.* In Chapter 2 we will show a simple derivation of Terzaghi's Law based on Archimedes' principle for solid particles suspended in a fluid.

There are many field evidences of Terzaghi's Law. It is the reason why the surface over oil fields subsides after hydrocarbon or other fluids are produced (Kugler, 1933; Gabrysch, 1967; Mayuga, 1970). In these examples (and there are many examples, such as the subsidence of the Ekofisk oil field in the Norwegian Sector of the North Sea and various offshore fields in the Gulf of Mexico and Louisiana, USA), the extraction of liquids led to a reduction in pore pressure, an increase in the effective stress (σ), and hence further compaction and subsequent subsidence of the reservoirs. In these cases, the reservoir pressure is *less* than the normal or hydrostatic pressure and gas and water are injected to counter the subsidence. In the case of Ekofisk Field, the drop in pore pressure was shown to be balanced by an increase of the effective stress in accordance with the Terzaghi's Law (Chapman, 1994a). Such effects can be monitored by 4D-seismic techniques (see Chapter 12).

1.6 Formation Pressure

As defined earlier, formation pressure is the pressure acting on the fluid contained in the pore spaces of sediments or rocks. Figure 1.1 illustrates a typical geopressure versus depth profile. The geopressure regime could be loosely classified in three zones: Subnormal or subpressure where pore pressure is below hydrostatic pressure; hydrostatic or normal pressure; and overpressure where the pore fluid pressure is higher than the hydrostatic pressure. The transition from hydrostatic to overpressure may be fairly well-defined as in the Miocene sections of the Texas–Louisiana Gulf Coast, or gradual as in the case of deepwater Pliocene and Pleistocene sections of the many Tertiary Clastic provinces in the world. The depths at which these transitions occur and the shape of the transition zone depend mostly on the permeability (it controls the fluid flow out of the sediments) and the rate of deposition of the sediments (it provides the source of the fluid in the sediments). Typically when the *outflow* of fluids (brine) is less than the *inflow*, the system is overpressured as the fluid begins to support the load. This mostly dictates the magnitude and the distribution of pore pressure. The extent of the transition zone can vary from a few hundred feet to many thousands of feet. Although there is no universally accepted scale expressing the degree of geopressuring, the nomenclature introduced by Dutta (1987a, Table 1, p. 5) is commonly accepted. This is reproduced in Table 1.4.

An important concept seen in Figure 1.4 is that pore pressure typically *does not* reach overburden stress. As pore pressure approaches overburden stress (actually, the least principal confining stress which is usually less than the overburden stress as discussed in Chapter 2), fractures in the rock open and release fluids and pressures. The pressure at which this happens is termed as the "fracture pressure." Thus, every rock has a characteristic limit defined as the *seal limit* in Figure 1.4. Fracture pressure at a given depth divided by the depth is known as the fracture gradient at that depth. There

Table 1.4 Geopressure characterization

Fluid pressure gradient (psi/ft)	Overpressure characterization
Hydrostatic $< FPG \leq 0.65$	Soft or mild
$0.65 < FPG \leq 0.85$	Moderate
$FPG > 0.85$	Hard

are three *important* quantities that the drilling community is mostly concerned with prior to drilling a well. These are*: pore pressure gradient, fracture gradient and overburden gradient.* All gradients are typically converted to EMW and the drilling plan deals with obtaining these quantities for the entire well.

Variation in the effective stress is also shown in Figure 1.4. It is the difference between overburden or lithostatic stress and pore pressure, i.e., essentially the amount of overburden stress that is supported by the porous network of rock grains as is allowed by the Terzaghi (1923) principle. If we assume that the pore fluid consists of brine with the density of 1.07 gm/cc (equivalent to a pressure gradient of 0.465 psi/ft), the normal or hydrostatic fluid pressure (in psi) will be given by

$$p_h = 0.465(\text{psi/ft})z(\text{ft}) \tag{1.14}$$

In this case, the effective stress (σ) will be given by

$$\sigma = 0.535(\text{psi}/ft)z(\text{ft}) \tag{1.15}$$

if we assume an overburden stress gradient of 1.0 psi/ft (i.e., equivalent to an assumed average and constant bulk density of 2.31 gm/cc). Hubbert and Rubey (1959) defined a quantity, λ, as the ratio between the formation pressure and the vertical overburden stress given by

$$P = \lambda\, S \tag{1.16}$$

Then,

$$\sigma = (1 - \lambda)\, S \tag{1.17}$$

Some authors (e.g., Fertl, 1976) used $\lambda = 0.9$ as an estimate of the upper limit of pore pressure in regressive sequences such as in the Tertiary rocks in the Gulf of Mexico, USA. They suggested that beyond this limit (seal limit) hydraulic fracture of the sedimentary rocks was a distinct possibility. Some practitioners use this as a measure of fracture pressure. However, the subject of subsurface fracturing due to overpressure (a natural cause) is more complex and it depends on many other factors besides pore pressure, such as lithology and tectonic stress and its orientation (Zoback, 2007). We shall discuss this in more detail in Chapter 2. Hubbert and Rubey (1959) also introduced a useful concept – *equilibrium depth* Z_E. This is defined as the depth where the effective stress is equal to what it would be at a shallower depth, had the rocks compacted normally. Swarbrick et al. (2002) introduced the term *fluid retention depth* (FRD) – it is the depth at which pore pressure begins to get higher than the normal pressure; it is also the depth where the effective stress (σ) reaches its maximum value (see Figure 1.4). We note that as pore pressure increases, so does the drilling time, cost and risk.

Overpressure implies low effective stress – lower than the effective stress for hydrostatic pressure conditions. Thus, it is maximum at the depth where the departure from hydrostatic to overpressure occurs. Drilling experiences have shown that the lowering of the effective stress in the overpressured zone is not “sharp” – it is typically preceded by a zone of almost constant effective stress. This has to do with various competing pressure mechanisms for generating geopressure as we shall see later in Chapter 3. The variables required for predicting and assigning prospect risks for prospectivity of hydrocarbons are (see Figure 1.4)

- the depth of the top of the overpressured zone,
- the depth of the top of the "hard overpressured" zone,
- the shape of the transition zone, and
- seal failure limit (the pressure needed to induce hydraulic fracturing of the "seal or cap rocks").

Let us consider the geometry of a brine-filled reservoir as shown in Figure 1.5. The reservoir is truncated at a fault and we assume that the fault is a sealing fault, namely, it does not allow any fluid to flow across the fault. In the absence of fluid flow, the difference in pore pressure between points A and B is simply the weight of the fluid in the vertical reservoir column (Figure 1.5a). If this fluid is water, pore pressure at any elevation in the reservoir will follow a hydrostatic slope as shown in Figure 1.5b. If the reservoir is overpressured and filled with brine, pore pressure will track a line parallel to the normal hydrostatic pressure curve for brine, which means that overpressure at each depth is the same as shown in Figure 1.2. This is important because it means that overpressure in a continuous reservoir unit must be constant throughout the water-bearing portion of the reservoir. This situation occurs because the permeability of the reservoir sand is much higher than that of the encasing impermeable rock (shale). In Figure 1.5, the pore pressure at the updip location (B) is related to the pore pressure in the downdip direction (A) by

$$P_A = P_B + (Z_A - Z_B) g \rho_f \tag{1.18}$$

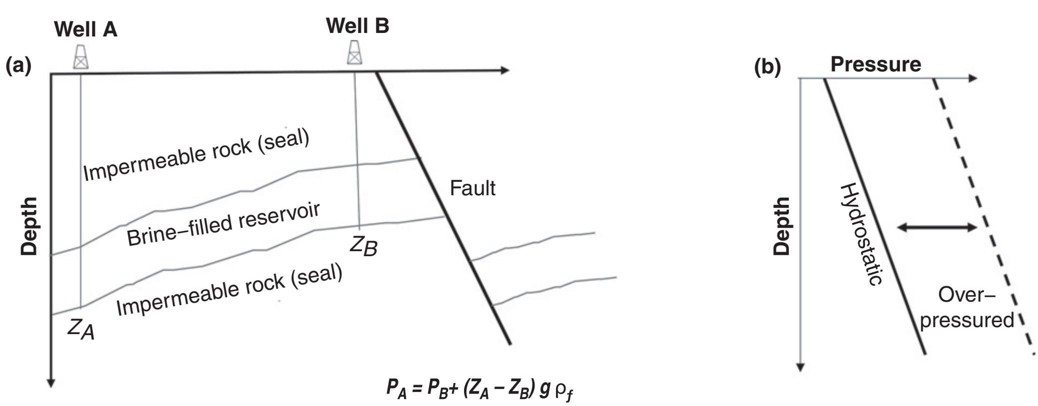

Figure 1.5 (a) Pore pressure profile of a reservoir sand with structure embedded in an overpressured shale. (b) For an overpressured sand filled with brine, the pore pressure tracks a line parallel to the normal hydrostatic pressure curve for brine.

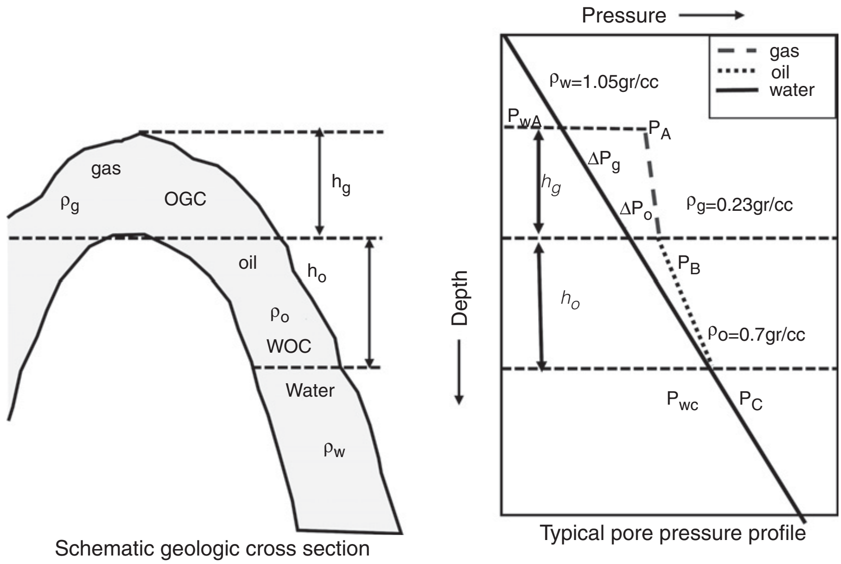

Figure 1.6 Schematic of a reservoir saturated with gas, oil, and water (left) and pore pressure elevated by oil and gas columns and density contrast between water, oil, and gas in a reservoir. Typical density contrasts are given in the figure on the right. (left) A hypothetical geologic cross section. (right) Pore pressure elevated by hydrocarbon columns in a hydraulically connected formation as depicted in cross section on the left. Modified after Zhang (2011).

In Figure 1.6 we show on the left a schematic geologic cross section of a hydraulically connected reservoir filled with gas of column height h_g, oil of column height h_o and brine. The right figure shows pore pressure elevated by hydrocarbon columns. This pressure profile is due to the buoyancy effect of the fluids. Typical values of fluid densities are 1.05 g/cm^3 for water (brine), 0.7 g/cm^3 for oil, and 0.23 g/cm^3 for gas as indicated by the slope changes of the pressure profiles on the right. It is clear from equation (1.18) and the buoyancy effect of hydrocarbons that at the crest of the structure, the pore pressure gradient would be larger than the case when the reservoir was brine saturated. This increases the possibility of the caprock failure. It is for this reason, drillers usually do not spud a well directly at the crest of a structure.

1.6.1 Subpressure

Subpressure formations are those in which the pore pressure is below the hydrostatic pressure. Such pressure conditions are known to exist in many depleted oil reservoirs, in areas with withdrawal of ground water and attendant local subsidence and in lenticular reservoirs closely associated with shales in areas that have undergone erosion. Since pore pressure gradient is datum dependent, the local topography plays a significant role. Pressure gradients can be either lower or higher than the hydrostatic pressure gradient.

In Figures 1.7a–c, we show three possibilities where the outcrop elevation and the well site elevation determine the pore pressure gradient as measured in that well bore. Figure 1.7a shows the normal pressure situation where the well elevation is the *same* as the outcrop elevation. The pressure gradient at the wellbore is 0.465 psi/ft (0.0105 MPa/m). Figure 1.7b shows the abnormally high pore pressure situation where the well elevation is *lower* than the outcrop elevation. The pore pressure at the wellbore is 0.465 psi/ft × 13,000 ft = 6045 psi (41.6787 MPa), leading to a pressure gradient of 6045 psi/10,000 ft = 0.6045 psi/ft (0.01360 MPa/m). Figure 1.7c shows a situation where abnormally low or subnormal pressure occurs where the well elevation is *higher* than the outcrop elevation. In this case, the pore pressure at the well site is 0.465 psi/ft × 7000 ft = 3255 psi (22.4483 MPa) leading to a pressure gradient of 3255/10,000 ft = 0.3255 psi/ft (0.007323 MPa/m) which is lower

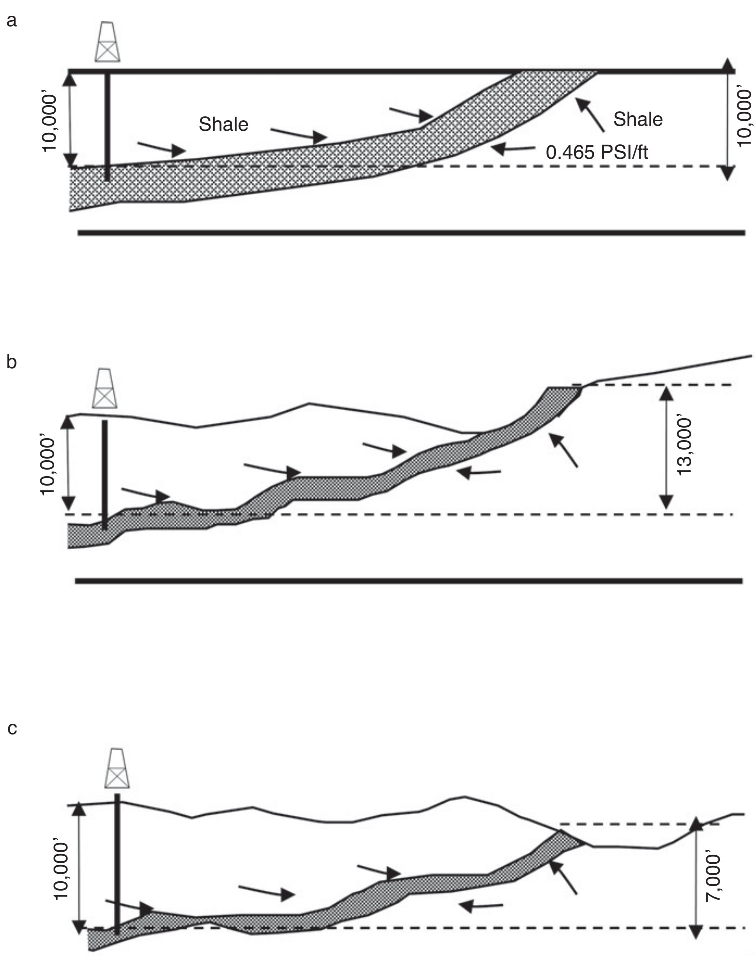

Figure 1.7 Effect of datum on pore pressure gradient. (a) Well elevation is the *same* as that of the outcrop elevation. (b) Well elevation is *lower* than the outcrop elevation leading to an abnormally high-pressure gradient. (c) Well elevation is *higher* than the outcrop elevation, leading to an abnormally low-pressure gradient.

than the normal pressure gradient. We note that subpressures are relatively uncommon except for depleted reservoirs. Proximity to a mountain range is also a feature that relate to subpressures – it provides a sink through which water is abstracted from the basins.

1.6.2 Fracture Pressure

In oil field terminology, fracture pressure is the pressure that causes a formation to fracture and the circulating fluids to be lost. Normally it is expressed as the fracture gradient or the fracture pressure divided by the depth. In this way, it determines the maximum mud weight that can be used to drill a well bore at a given depth. Hence it is an important parameter for mud weight design in both the drilling planning stage and in the drilling stage. If the mud weight is higher than the fracture gradient of the formation the well bore will undergo tensile failure, causing losses of drilling mud or even lost circulation. In practice, fracture pressure is measured from various types of leak-off tests (LOT). A leak-off test is performed to estimate the maximum amount of pressure or fluid density that the test depth can hold before leakage and formation fracture may occur. This measurement is usually made at the casing points. There are several approaches to calculate fracture gradient. We shall discuss this in details later (Chapters 2 and 4).

1.6.3 Equivalent Circulation Density (ECD)

This is an important concept in drilling. Hydrostatic weight of the mud is intended to balance the formation pressure under "static" condition. During drilling, mud pumps are turned on and the situation is no longer static. In this case, the borehole geometry introduces *pressure loss* based on drag on the fluid as it passes through the various components of the fluid flow path during drilling such as standpipe, drillstring components, open hole, and casing. The mud pumps supply the pressure that forces drilling mud down the drill string to the bottom of the hole and up again to the surface. As the drilling mud exits the bit nozzles, the mud has to flow through the annular space between the drill string and the borehole wall. Contact is made between the drilling mud and the borehole wall as the drilling mud flows upward to the surface. This contact creates "drag" as the result of friction and the drilling mud loses some of the pressure supplied by the pump in order to overcome this frictional drag. This pressure loss is absorbed by the formation. Equivalent circulating density (ECD) is the effective density that combines current mud density and annular pressure drop. Thus, ECD in ppg = (annular pressure loss in psi) ÷ 0.052 ÷ true vertical depth (TVD) in ft + (current mud weight in ppg). This is why the ECD is always *greater* than the mud density under static condition. The greater the vertical distance through which the drilling mud has to travel until it reaches the surface, the higher are the pressure drop and ECD. Note that ECD is a function of the *true vertical depth* and *not the measured depth*. Measured depth includes the horizontal section in deviated wells but ECD only depends on the true "vertical" depth. Acquired solids (cuttings), the type of mud and its temperature also affect ECD.

1.7 Casing Design

Both pore pressure and fracture pressure dictate the casing design in drilling. A casing is a large heavy steel pipe which is lowered into the well. Generally, a casing is subjected to various physical and chemically related loads during its lifetime. Its purpose is to prevent collapse of the borehole while drilling, hydraulically isolate the wellbore fluids from formations and formation fluid, minimize damage of both the subsurface environment from the drilling process and from extreme subsurface environment, provide a high strength flow conduit for the drilling fluid, and provide safe control of formation pressure. If the casing is properly cemented it can also help to isolate communications between different perforated formation levels. Selection of the number of casing string and their respective setting depths generally is based on a consideration of the pore pressure gradients and fracture gradients of the drilling area. In Figure 1.8, we show a typical casing design for a hydrocarbon well.

A casing string consists of (1) surface casing, (2) intermediate casing, (3) liners, and (4) production casing. The main purpose of the surface casing is to prevent the shallow water region from contamination, the structural support for weak soil areas near the subsurface, and also protect the casing strings inside. Again, this can prevent blowout and can close the surface casing in the event of a kick or explosion. When drilling

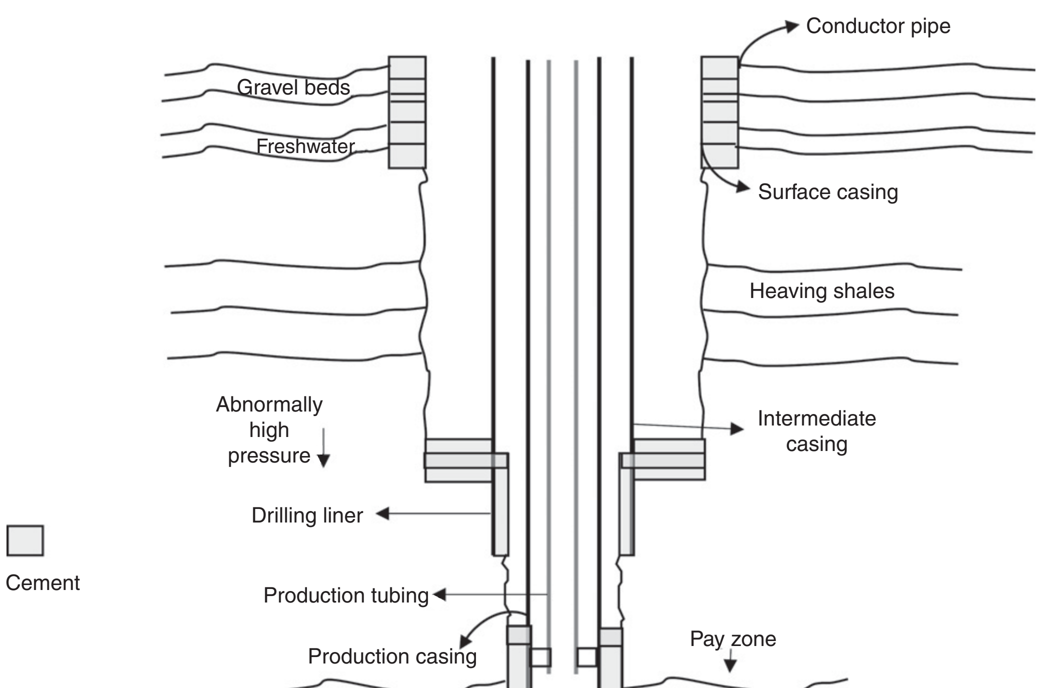

Figure 1.8 Typical casing strings used in the hydrocarbon industry. Modified after https://petrowiki.org/o_and_tubing.

deeper through weak zones like salt sections and abnormally pressurized formations, these unstable sections need more pipe sections, in the form of intermediate casings between the surface casing and the final casing. When abnormal pore pressures are present below the surface casing, intermediate casings are needed to protect the formation. The liner is a casing string that does not extend to the surface. It is suspended from the bottom of the next large casing string. The principal advantage of a liner is its lower cost. It serves as a low cost intermediate casing. This casing string provides protection for the environment in the event of a failure during production. Generally, there are two types of wells. The first are exploration wells that are drilled and abandoned within a few months. The second are production wells that are used continuously through their life. Production casings are connected to wellhead using a tie-back when the well is completed. This casing is used for the entire interval of the drilling.

Drilling environments often require several casing strings to reach the total desired depth. Some of the strings are: drive, or conductor, surface, intermediate (also known as protection pipe), liners, and production (also known as an oil string). Figure 1.8 shows the relationship of some of these strings. All wells will not use each casing type as shown. The conditions encountered in each well must be analyzed to determine types and amount of pipe necessary to drill it. Pore pressure and fracture pressure are the two most important parameters that dictate the casing design. For example, selecting casing seats for pressure control starts with formation pressures (expressed as EMW) and fracture – mud weight. This information is generally needed prior to designing a casing program. Quantitative evaluation of geopressure is essential to determine the exact locations for each casing seat. This procedure is implemented from the bottom to the top as shown in Figure 1.9. Setting-depth selection is made for the deepest strings to be run in the well, and successively designed from the bottom to the surface. Although this procedure may appear at first to be reversed, it avoids several time-consuming iterative procedures. Errors in estimates of pore pressure and fracture pressure affect the casing design significantly. Surface casing design procedures are based on other criteria also, such as shallow hazards. We shall discuss this in Chapter 11.

As noted earlier the first criterion for selecting deep casing depths is for mud weight to control formation pressures *without* fracturing shallow formations. It is a common practice to establish a “safe mud window” as shown in Figure 1.9. This window is typically 0.2–0.3 ppg *lower* than the fracture pressure and 0.2–0.3 ppg *higher* than the “anticipated” formation pressure. It is clear that as the well is drilled to deeper depths, the width of the “safe mud widow” will become narrower; this can cause a severe problem if the program is not managed properly. In Kankanamge (2013), readers will find an interesting case study in how to design a casing for a deep gas well.

1.8 Importance of Geopressure

Geopressure is a worldwide phenomenon as shown in Figure 1.10 where many of the formations are in overpressured conditions. There is a good description of these in Fertl

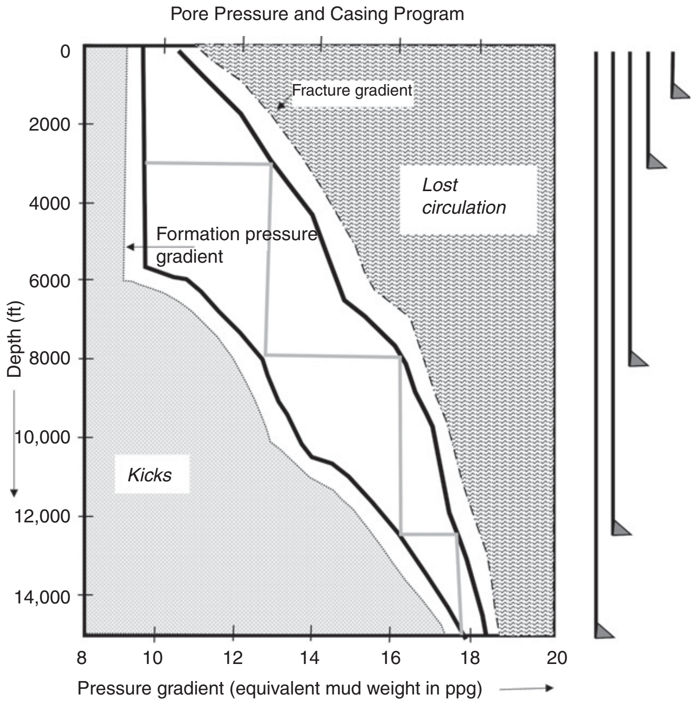

Figure 1.9 Pore pressure gradient versus depth and setting a casing program for a hypothetical well. Note that drillers use a safety margin prior to designing a casing program. It is typically 0.2–0.3 ppg higher than the formation pressure and 0.2–0.3 ppg lower than the fracture pressure gradient.

(1976), Chapman (1994b), and Chilingar et al. (2002). A quantitative study of geopressure is essential for the following reasons:

- guide safe drilling activity (proper mud and casing program and blowout prevention),
- provide exploration support for hydrocarbon (trap/risk identification and hydrocarbon migration path assessment; seismic imaging improvements; economic basement assessment), and
- assess environmental risks (shallow hazards identification and mitigation including overpressured aquifer sands and gas hydrates).

Most sedimentary basins exhibit characteristics of overpressured formations to varying degrees. Although overpressure is more pronounced in young basins, they are known to occur in formations with highly varied lithologies such as sandstone, shale, limestone, and dolomite anywhere between Pleistocene and Cambrian (Fertl, 1976; Law and Spencer, 1998). They are also known to occur in igneous environments such as in the Gulf of Bohai in China (Chilingar et al., 2002).

The United States Geological Survey sponsored a Conference on the Mechanical Effects of Fluids in Faulting under the auspices of the National Earthquake Hazards

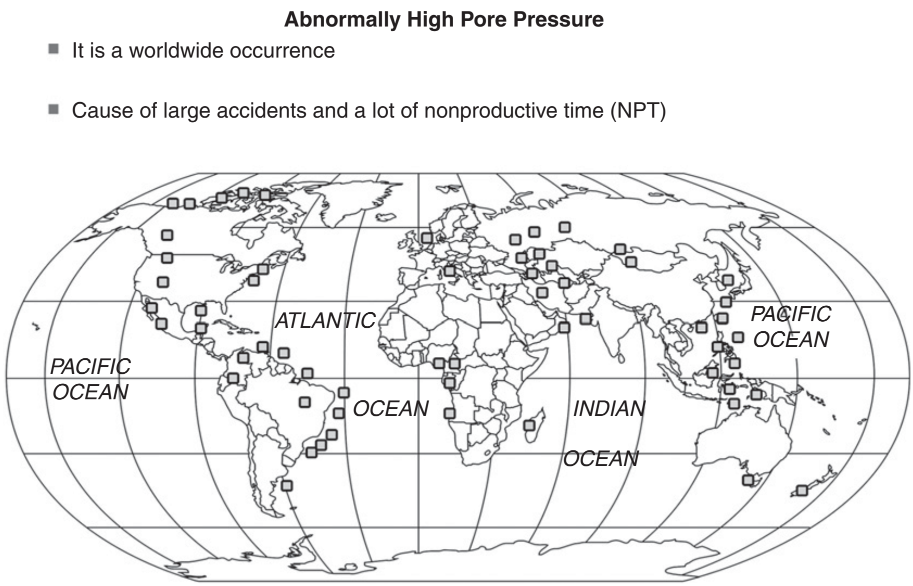

Figure 1.10 A world map showing occurrences of geopressure. It is a worldwide phenomenon. It causes big accidents and significant nonproductive time (NPT) during drilling.

Reduction Program at Fish Camp, California, from June 6 to 10, 1993. At that conference a growing body of evidence suggested that fluids were intimately linked to a variety of faulting processes (Hickman et al., 1995). The authors noted that these included the long term structural and compositional evolution of fault zones; fault creep; and the nucleation, propagation, arrest, and recurrence of earthquake ruptures. This is generally believed now. Occurrence of overpressure is not necessarily contemporaneous with the surrounding sediment. For instance, the presence of high pressured fluids in Paleozoic formation may have been developed in the Tertiary period. Fluid containment in a closed or semiclosed environment is the source of abnormally high pore pressure. It is for this reason that there is evidence of high pore pressure in thick Paleozoic shale formations in Wyoming (Hubbert and Rubey, 1959) and subsequent detachment and movement of some of the thick blocks of overpressured rocks from underlying formations. Thus, overpressures are intimately related to structural geology and it is found in various ages of formations.

1.8.1 Guide for Safe Drilling Practices

Even though the petroleum industry has a good safety record, drilling through high pressured formations is known to pose serious drilling challenges. Blowouts are also known to occur occasionally. Some of the reasons are listed above. While catastrophic events are rare, what is not rare is the nonproductive drilling time spent during a drilling operation as shown in Figure 1.11. About 95 percent of the incidents involves problems related to drilling performance. In addition, ~5–25 percent of the well cost is

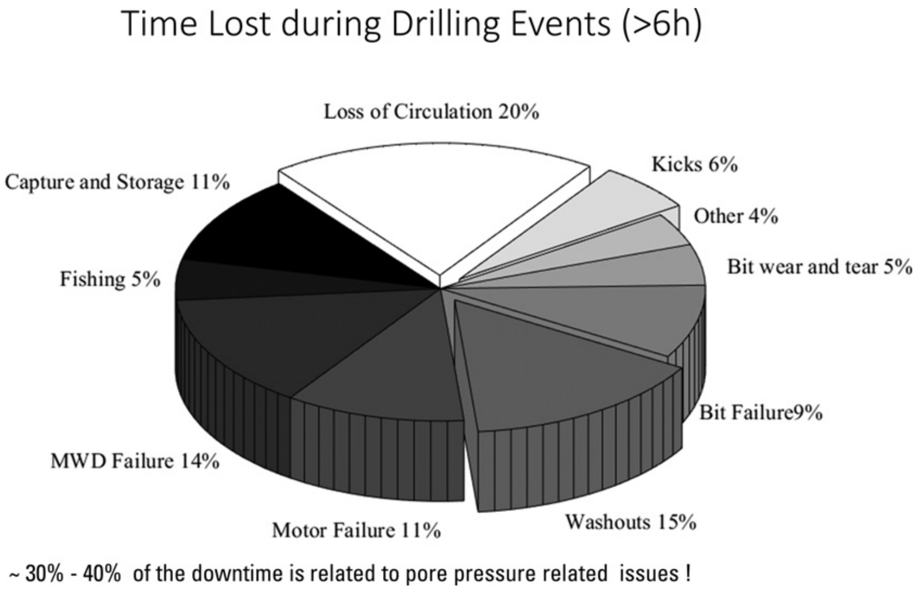

Figure 1.11 Time lost during drilling (nonproductive time or NPT) as known in the petroleum industry. About 30–40 percent of NPT are due to issues related to overpressure. *Fishing* is a term used by the driller to retrieve any tool lost in a borehole.

a result of inadequate drilling performance. As the data shows, ~30–40 percent of the operations cost during drilling are related to overpressure. Some estimates put the total loss to the industry as high as $3.0 billion annually. For serious problems such as those due to loss of circulation of drilling mud into the surrounding formation or influx of the formation fluid into the borehole (Figure 1.11), the nonproductive downtime could be as long as seven days or higher – for deepwater drilling activities where daily rig rates could be as high as $200 million, the losses could be very high. In the extreme case, if the formation pressure encountered during drilling is much higher than planned, it would be impossible to drill through to the target at deeper depths and to set proper casing as there may not be enough casing string left. This would result in abandoning the well without reaching its target and thus causing huge losses.

We mentioned earlier that quantitative analysis of geopressure is important as it impacts the *mud program* while drilling a well. Mud program refers to designing a formal plan for drilling fluid requirements in general and specific maintenance need, namely, choosing drilling fluid for a specific well with predictions and requirements at various intervals of the wellbore depth. It consists of details on the mud type; composition, density, rheology, filtration and other properties. The density is especially important because they must fit with the casing design program and to ensure wellbore pressures are properly controlled as the well is drilled deeper. Good drilling fluid or mud (as is known in the industry) with proper density is necessary to ensure that no formation fluid influx occurs into the wellbore. This is particularly important while drilling in high pressured wells that require increasing the fluid density (or mud weight) with depth. However, a best practice dictates that the drilling fluid density or the mud weight must not be too high as compared to the true formation pressure. If not, it can cause a serious drilling problem known as lost circulation with unwanted consequences such as formation of thick mud filtration between the well bore and the formation, poor cementing job, and so on. (There are other uses of a good drilling fluid: remove cuttings expeditiously from beneath the drill bit; transport cuttings to the surface without degradation; economically deliver a wellbore suitable for formation evaluation and completion and control torque on drill string, particularly in deviated wells.) Thus, variation of geopressure with depth is perhaps the key parameter that dictates designing a good mud program.

There is another importance of geopressure that impacts safety. As we will learn in this book that high pressures usually occur in thick shale formations with considerably higher water (brine) content compared with the normally pressured case. The types of drilling fluid used depend on the pressure regime. In the low-pressure regime, cost-effective water-base drilling fluid (with bentonite mud) is commonly used. For higher pressured wells, the industry uses oil-base drilling fluid. It is expensive and affects the rate of penetration of the drill bit. Thus, a transition from water-base mud to oil-base mud at a specific depth is highly influenced by the details of the quantitative profile of geopressure with depth.

1.8.2 Exploration Use

In the context of exploration for hydrocarbon, a proper quantification of pore fluid pressure in 3D is highly desirable as it can suggest a path for hydrocarbon migration through porous formations and subsequent trapping, either stratigraphically or structurally favored environments (faults, folds, etc.). Thus, the hydrodynamics of a sedimentary basin is greatly impacted by the distribution of pressured fluids, and an analysis may reveal the proper location to drill (or to avoid) and the expected height of hydrocarbon column in the prospect area. The economics of drilling for hydrocarbon is impacted in two major ways by the presence of overpressure in sedimentary basins. First, one would like to know the depth of an economic basement, if any. This is defined as the depth where the pore pressure is so high (and the vertical effective stress is so low) that the likelihood of fracturing the rock by natural causes such as hydraulic fracturing or rock movement due to earthquake can cause the hydrocarbon trap to mitigate and the oil and gas accumulation to escape from the reservoir. Figure 1.12, developed for a part of the Gulf of Mexico (Dutta, 1997b), shows such a map in which color codes indicate potential areas of possible *seal failure* due to high pore pressure. Each square block of that figure represents a federal lease area – a block that is 9 sq mi. The red colors indicate areas with possibility of low effective stresses (~500 ± 250 psi). Maps such as the one in Figure 1.12 could be used to high-grade the prospect inventory (possibility of seal mitigation) and assign a potential hazard index to those areas with extremely *low* effective stresses for drilling. Second, the explorer of hydrocarbons would like to know the depth of the *top* of the onset of overpressure (Figure 1.13) and the distribution of overpressure in 3D (Figure 1.14). As we shall see

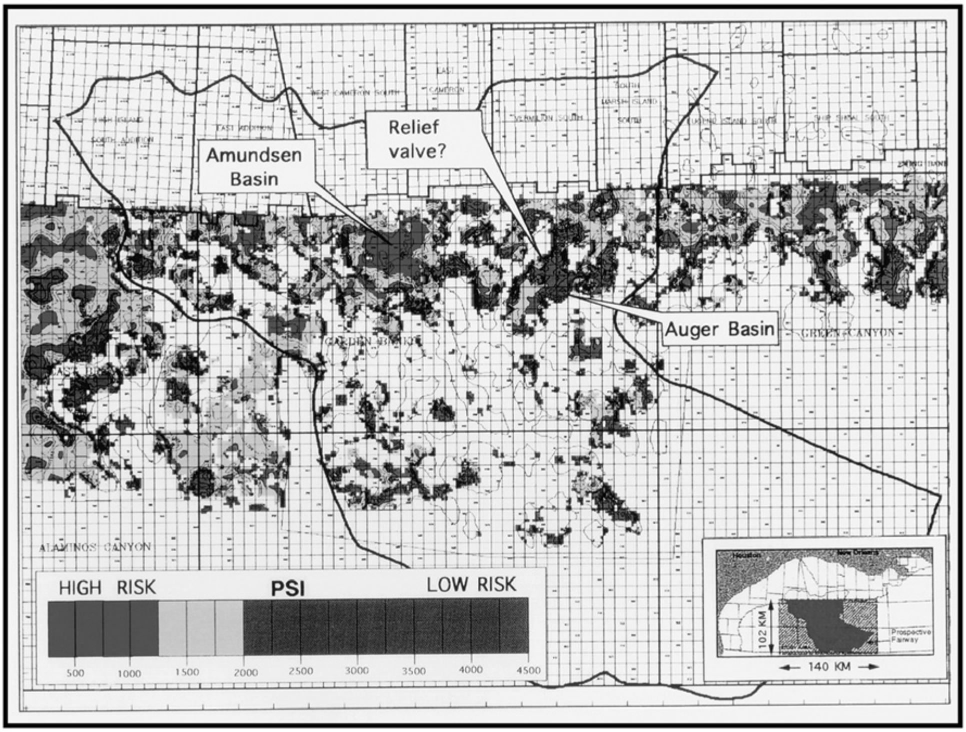

Figure 1.12 Effective stress and seal failure map in a large area of the Gulf of Mexico (see inset) as predicted from a combination of surface seismic and basin modeling. Red indicates high probability of seal failure. Taken from Dutta (1997b). The range of effective stress is from 0 to 5000 psi. (A black and white version of this figure will appear in some formats. For the color version, please refer to the plate section.)

later, the hydrocarbon column height in a reservoir is greatly impacted by the magnitude of overpressure in the reservoir – *higher* the overpressure, the *lower* will be the total hydrocarbon column height. This is because the buoyancy force due to hydrocarbon will contribute further to the existing high pore pressure of the fluids, thus raising the likelihood of *seal leakage* and eventually *seal failure.*

Recent studies have indicated another use for quantification of geopressure for exploration. This is related to defining a better seismic velocity model for seismic imaging. Traditionally, seismic velocities are obtained by various inversion processes (we will study this in Chapter 5) that produce velocity models that are inherently nonunique and potentially ambiguous. Recent studies (Dutta et al., 2014, 2015a, 2015b; Le et al., 2018) have shown that imposing a pore pressure *constraint* on the derived seismic velocity model and demanding that the velocity model yield a *physically plausible* pore pressure model, namely, the predicted pore pressure be equal or higher than the hydrostatic pore pressure and be less than the fracture pressure, for example, yields a better seismic image of the subsurface. An example is provided in Figure 1.15. Figure 1.15a shows the legacy image using conventional velocity analysis (tomography based anisotropic velocity analysis) while the one in Figure 1.15b (that

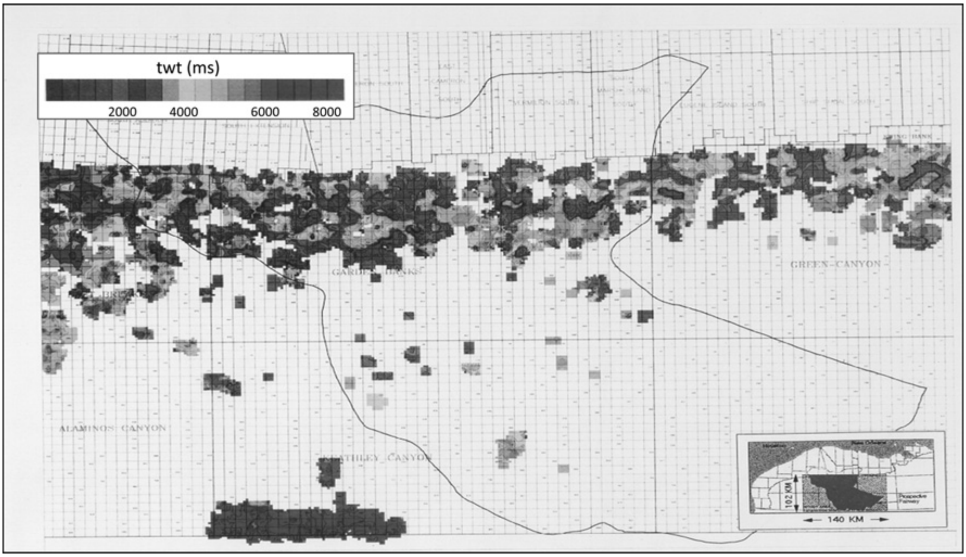

Figure 1.13 Two-way time to the top of overpressure for the same area as shown in Figure 1.12. Blue indicates shallow overpressure. Taken from Dutta (1997b). The scale is two-way time (twt); the range is 0-8000 ms. (A black and white version of this figure will appear in some formats. For the color version, please refer to the plate section.)

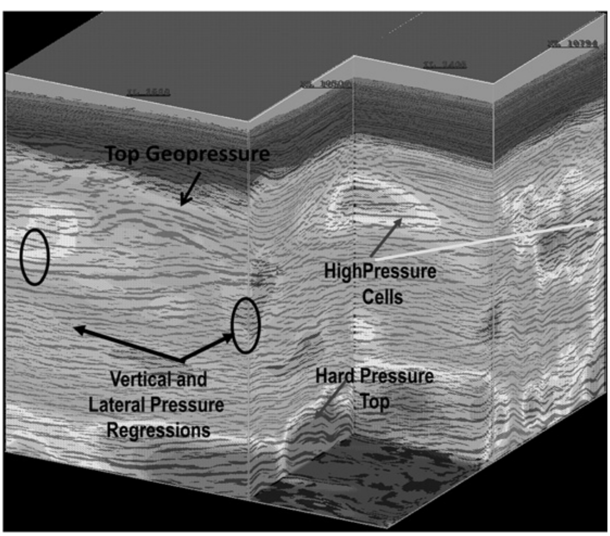

Figure 1.14 Seismic-based map of distribution of pore pressure in 3D. Annotation shows "sweet" spots for exploration and identifies areas for "drilling" through risky zones. The size of the cube is ~600 sq. mi. in area and 5 s deep (in time). From Dutta and Khazanehdari (2006). (A black and white version of this figure will appear in some formats. For the color version, please refer to the plate section.)

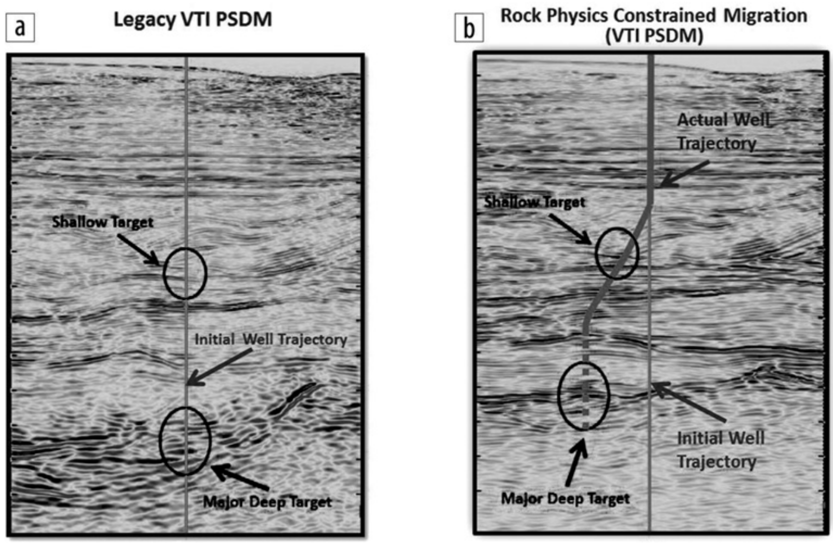

Figure 1.15 Use of seismic data to improve the image of subsurface formations in a velocity model. (a) An image based on a legacy anisotropic velocity model. (b) An improved image based on an anisotropic velocity model that uses pore pressure constraint on the velocity model. The image is better focused. This led to a better well path trajectory to reach the deeper target. After Dutta et al. (2014).

used a *constrained* anisotropic velocity model (tomography) – constrained by plausible range of pore pressure) shows a marked improvement. Not only is the velocity lowered (a consequence of high pore pressure) but the seismic energy is more focused resulting in a better illumination of the image of the potential deep targets for exploration. We shall discuss this approach for building a common velocity modeling for pore pressure and imaging in detail in Chapter 6.

Over the last several decades, our quest for hydrocarbon exploration and drilling has taken us to the frontiers of the deepwater where sizable accumulations have been found. These activities have pointed to a link between high pore pressures and potential risk to the environment. We have seen the risk of blowouts of pressured aquifer sands in the shallow part of the stratigraphy below seabed (Ostermeier et al., 2002). These are known in the industry as *shallow-water-flow* (SWF) *sands* – it is a deepwater phenomenon and deals with aquifer pressured sands held by a thin veneer of clay. Drilling through these sands can cause blowouts and serious damages to the environment. This is a near-surface geologic phenomenon and the quantification of pore pressure is difficult but necessary so that adequate precautions (avoidance, for example) can be undertaken. In Figure 1.16, we show a compilation of many other geological causes of geohazards – not all of which are related to high pore pressure. An example is the gas hydrates in deepwater that exist in the environment similar to the place where SWF sands occur. In Chapter 11 we shall discuss how to quantify some of these geohazards and the role of geopressure.

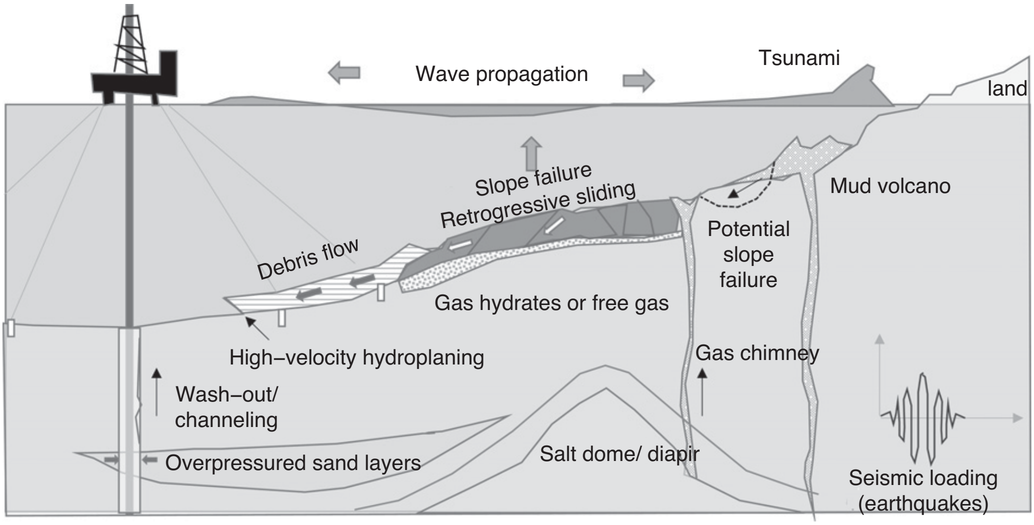

Figure 1.16 A schematic compilation of geological causes of geohazards.

1.8.3 Seals, Seal Capacity, and Pore Pressure

Hydrocarbon exploration is fundamentally about recognizing three things in a sedimentary basin: existence of source rocks (source), a reservoir or container for hydrocarbon to migrate into (reservoir), and a seal or a lid to contain the hydrocarbon (seal). Geopressure impacts all of these and in addition, it facilitates the primary and secondary migration of hydrocarbon (Tissot and Welte, 1978). In a scholarly article, Watts (1987) describes three types of seals: hydrodynamic, caprock, and fault. Hydrodynamic seals are controlled by excess hydrodynamic head above hydrocarbon accumulation. In this case hydrocarbon column reaches equilibrium when hydrocarbon buoyancy pressure is balanced by a downward hydrodynamic flow force, as shown in a schematic diagram in Figure 1.17 in an anticlinal reservoir under the condition of increasing action of flowing water (brine). Under hydrostatic conditions (no flow), oil and gas would simply rise (top figure), according to the principle of buoyancy, to the highest available part of the trap. Under hydrodynamic conditions, however, it is not necessary that hydrocarbon (oil or gas) rises in the crest position of the structure. Fault-related seals are those that prohibit fluid migration through the faulted regions and these are controlled by the entry pressure of largest interconnected pore throats across the fault planes. Sealing faults are caused mainly by clay smear (very low permeability) or a variety of diagenetic processes (Tissot and Welte, 1978).

In the petroleum industry, *caprock* is defined as any nonpermeable formation that may trap oil, gas or water, thus preventing it from migrating to the surface. Caprock is essential to create a reservoir of oil, gas or water beneath it and is a primary target for the petroleum industry. It can be overpressured as is the case for almost all Tertiary Clastic basins. According to Tissot and Welte (1978), caprock seals can be of two types: *membrane and hydraulic*. The membrane seal integrity is mostly controlled by

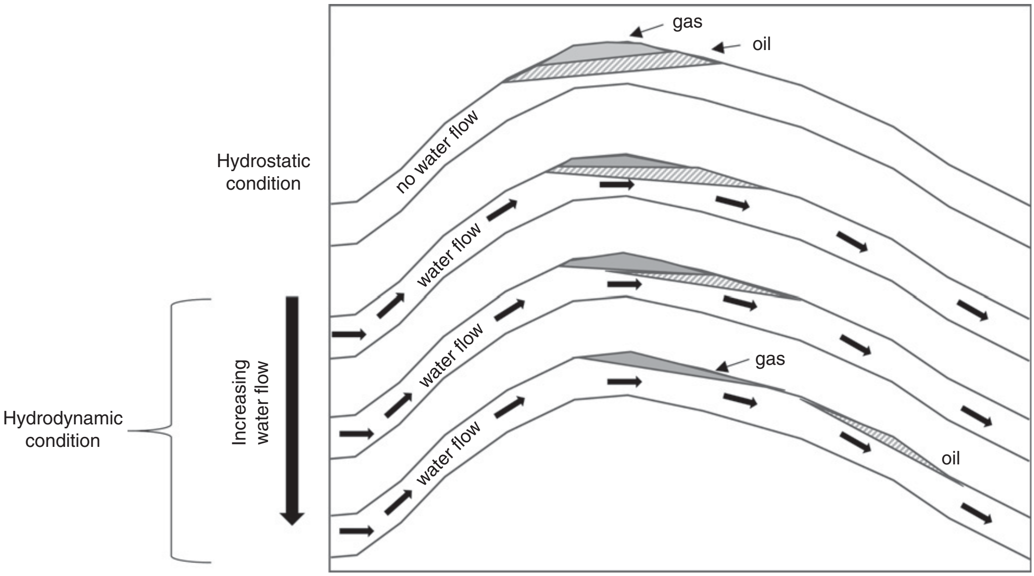

Figure 1.17 Hydrocarbon distribution in an anticlinal reservoir under the conditions of increasing action of flowing water (brine). Modified after Tissot and Welte (1978).

the entry pressure of largest interconnected pore throats, while this is not the case for hydraulic seals where seal breach occurs mainly due to hydraulic fractures (typically due to high overpressure).

Seal capacity refers to the hydrocarbon column height that the caprock can retain before capillary forces allow migration of the hydrocarbon into, and possibly through, the pore system of the caprock. Seal capacity is affected by both the physical properties of seal including its pore pressure state and the properties of the hydrocarbon. When hydrocarbon begins to fill in a reservoir, the pore space of that reservoir is usually filled with water (formation water). As hydrocarbon has a lower density than the formation water occupying the pore space, the hydrocarbon rises upward through the reservoir due to buoyancy (the density difference between hydrocarbon and water). Greater the density difference between the two phases is, so is the buoyant force that pushes the less dense, more buoyant hydrocarbon-phase upward.

The upward movement of the hydrocarbon through the pore system is resisted by capillary pressure. Capillary pressure is defined as the pressure required to displace the formation water from the pores and pore throats of the seal. The capillary pressure P_c is known as the displacement pressure in the petroleum industry, and it is given by (Berg, 1975)

$$P_C = \frac{2\gamma \cos\theta}{r} \tag{1.19}$$

where γ is the interfacial tension (dynes/cm) between hydrocarbon (oil or gas) and brine, θ is the contact angle (degrees), and r is the pore throat radius (cm). Clayton and

Hay (1994) showed the following relation for the thickness of the hydrocarbon column T_H:

$$T_H = \frac{2\gamma \cos\theta}{r(\rho_w - \rho_h)g} - \frac{\Delta P}{(\rho_w - \rho_h)g} \tag{1.20}$$

where ρ_w is the density of the formation water (brine), ρ_h is the density of the trapped hydrocarbon, g is the acceleration due to gravity, and ΔP is the overpressure in reservoir *relative* to the seal (caprock). The first part of the right-hand side of equation (1.20) gives the column height under normal or hydrostatic pore pressure conditions (seal capacity), and the second part gives a correction for excess reservoir overpressure. In Figure 1.18 we show the range of seal capacities of different rock types as documented in AAPG Wiki. This figure was compiled from published displacement pressures based upon the mercury capillary curves. Column heights were calculated using a 35°API oil at near-surface conditions with a density of 0.85 g/cm^3, an interfacial tension of 21 dynes/cm, and a brine density of 1.05 g/cm^3. Data were compiled from Smith (1966), Thomas et al. (1968), Schowalter (1979), Wells and Amaefule (1985), Melas and Friedman (1992), Vavra et al. (1992), Boult (1993), and Shea et al. (1993). The figure suggests that (1) shales can trap thousands of feet of hydrocarbon (normally pressured case), (2) most clean sands can trap up to 50 ft or less column of oil, and (3) poor quality sands and siltstones can trap 50–400 ft of oil. Carbonates have a wide range of displacement pressures. Some carbonates can seal as much as 1500–6000 ft of oil.

We note that higher the overpressure, lower is the hydrocarbon column height. This is clear from the following:

$$H_{hc,\max} = \frac{FP - RP}{(\rho_w - \rho_{hc})g} \tag{1.21}$$

where

$H_{hc,\max}$ = maximum hydrocarbon column height
FP = fracture pressure or the pore pressure at which hydraulic fracturing occurs
RP = reservoir pressure or the pore pressure of the brine-filled reservoir
ρ_w = density of brine
ρ_{hc} = density of hydrocarbon

The fracture and reservoir pressure should be estimated or measured at the crest of the structural closure. Equation (1.21) shows why a study of geopressure is so important – as reservoir pressure increases (due to some overpressure mechanisms), the hydrocarbon column height decreases. It impacts both hydrocarbon accumulation and migration from source to reservoir. It also defines the seal integrity of caprock, namely, whether hydraulic fracture would occur or not. Compaction and diagenesis during burial cause a progressive reduction in pore throats in most seal lithologies. This affects seal capacity. In addition, the interfacial tension of the hydrocarbons changes

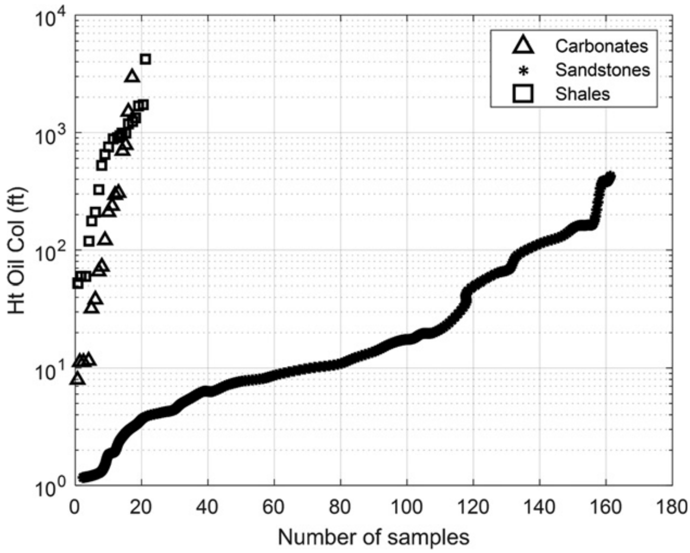

Figure 1.18 Range of measured seal capacities of oil accumulation for different rock types. Modified after a figure from the AAPG Wiki at http://wiki.aapg.org/Seal_capacity_of_different_rock_types.

with depth and affects seal capacity. Most importantly, the interfacial tension of oil and gas changes at different rates and impacts the seal capacity.

1.8.4 Permeability and Fluid Flow in Porous Rocks

Rocks are porous material composed of solid grains, void spaces and fluids in the void spaces. Darcy (1856) showed that the fluid flow rate in a porous rock is linearly related to the pressure gradient. The flow equation can be expressed generally as

$$Q = -\frac{\kappa A}{\mu} gradP \tag{1.22}$$

where Q is the vector fluid volumetric velocity, A is the cross-sectional area normal to the pressure gradient, μ is the fluid viscosity, and κ is the permeability (it is a tensor) with units of area. The unit of permeability commonly used is Darcy. We shall discuss how permeability affects fluid flow and contributes to geopressure in Chapter 3 in detail. The ability of fluids to flow is controlled by the permeability κ that is of great importance in the petroleum industry. Formations that transmit fluids readily, such as sandstones, are described as permeable and tend to have many large, well-connected pores. Impermeable formations, such as silts and shales, tend to be finer grained or of mixed grain sizes, with smaller, fewer, or less interconnected pores. *Absolute permeability* is defined as that permeability measured when a single fluid is present in the rock. Its dimension is of an area. *Relative permeability* is the ratio of permeability of a particular fluid at a particular saturation to the absolute permeability of that fluid at full saturation. It is a dimensionless quantity. Calculation of relative permeability enables us to compare different abilities of each fluid to flow in the presence of the other. The presence of more than one fluid generally hinders flow. *Effective perm*eability is a measure of permeability when two immiscible fluids occupy the same pore space of a rock, the movement of each is influenced by the other, and by their saturations. The following are the typical ranges of the individual permeability of common rock types:

Conventional oil and gas reservoirs ~ milli-Darcy (10^{-3} Darcy)
Tight sands, coal and some shales ~ micro-Darcy (10^{-6} Darcy)
Some coals and most shales ~ nano-Darcy (10^{-9} Darcy)

Permeability of sediments is related to porosity ϕ and therefore, it will decrease with compaction as rocks are buried. The Kozeny–Carman equation (Kozeny, 1927; Carman, 1937) describes the relationship between permeability κ, porosity, and grain diameter d, as follows:

$$\kappa = B \frac{\phi^3}{(1-\phi)^2} d^2 \tag{1.23}$$

where B is a constant that includes tortuosity of the rock. The porosity exponent of 3 in equation (1.23) is valid for very clean sandstones. Higher exponents are more appropriate of clays and shales (Bourbie et al., 1987).

In this chapter we introduced a host of definitions related to pore pressure and drilling. In Appendix B the readers will find a glossary of some of the commonly used terms introduced in this chapter as well as those used in the industry.

2 Basic Continuum Mechanics and Its Relevance to Geopressure

2.1 Introduction

Geopressure treatment relies on the joint analysis of stress and pore pressure. As our concern here is the treatment of the macroscopic behavior of earth materials, the continuum approach is appropriate to the analysis of both fields within the earth. Therefore, we begin by reviewing basic concepts and defining the general mathematical and physical entities used in the analysis and study of stresses and strains in a continuum. We then review some concepts of poromechanics – continuum mechanics applied to porous materials – that are relevant for understanding stresses and pore pressure in fluid-filled rocks and sediments in the earth. We provide here some results that can be reviewed in more detail in specialized books on the subject, such as Malvern (1969). We end the chapter with a discussion on the relevant rock physics basis for detection and estimation of geopressure.

2.2 Stresses and Forces in a Continuum

2.2.1 The Continuum Concept

When we are not concerned about the molecular structure of matter, we need a macroscopic explanation for the behavior of the material. Thus, we assign properties to the material as if it is continuously distributed throughout the volume of interest and completely fills the space it occupies. This *continuum concept* is a fundamental postulate in continuum mechanics.

Continuum Concept Example: Mass Density

The average density of a material is defined as

$$\rho_{av} = \frac{\Delta M}{\Delta V} \tag{2.1}$$

where ΔM is the mass contained within the volume ΔV. The density of the point in the continuum inside the volume is given mathematically (in accordance with the continuum concept) as

$$\rho = \lim_{\Delta V \to 0} \frac{\Delta M}{\Delta V} = \frac{dM}{dV} \tag{2.2}$$

2.2.2 Homogeneity, Isotropy

A *homogenous* material is one having identical properties at all points. With respect to one property, a material is *isotropic* if that property is the same in all directions at a point. A material is called *anisotropic* if those properties are directionally dependent at a point.

Tensors

We have seen that a physical law must be coordinate independent. A vector is a quantity that has a direction and magnitude in an $[x_1, x_2, x_3]$ system. To transform the vector **V** into a new coordinate system, we use the transformation matrix **Q**. The vector **V′** in the new coordinate system $[x'_1, x'_2, x'_3]$ is given by

$$\underline{V}' = \underline{\underline{Q}}\,\underline{V} \tag{2.3}$$

A vector can be defined as a first-rank tensor based on the transformation law of equation (2.3). A second-rank tensor will follow a transformation law of the form

$$\underline{\underline{\sigma}}' = \underline{\underline{Q}}\;\underline{\underline{\sigma}}\;\underline{\underline{Q}}^T \tag{2.4}$$

To better understand tensors of second and higher rank, we analyze stress as an example for a physical law that relates force at a point (traction) to the state of stress in the solid. It will be shown that the stress is a second-rank tensor. Higher-rank tensors will be introduced through the text as needed.

Cauchy's Stress Tensor

Two types of forces can act on an object: body forces, which act everywhere within the object, resulting in a force proportional to the volume of the object (e.g., gravity, inertia), and surface forces. The body forces are given by their relation to density or mass as

$$\underline{p} = \rho \underline{b} \;\; or \;\; p_i = \rho b_i \tag{2.5}$$

The vector **p** is force per unit volume and **b** is force per unit mass.

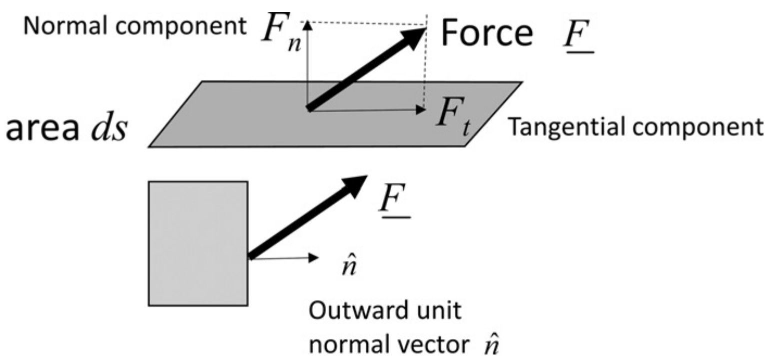

Figure 2.1 Forces acting on a surface.

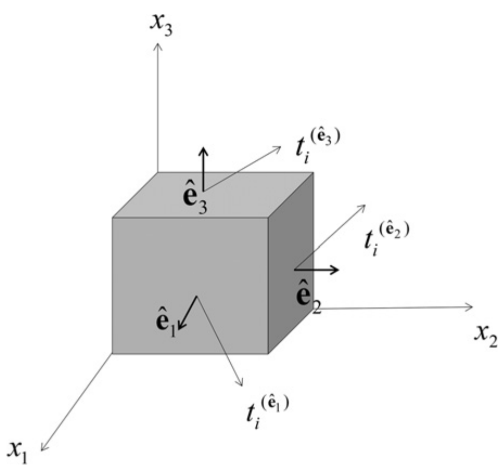

Figure 2.2 Traction forces.

Surface forces act on the surface of the volume, yielding a net force proportional to the surface area of the object.

We will define the surface forces as traction [force/unit area] as shown in Figure 2.1:

$$\underline{t}\,(\hat{n}) = \lim_{ds \to 0} \frac{\underline{F}}{ds}$$
$$t_i^{(\hat{n})} = \lim_{ds \to 0} \frac{F_i}{ds} \tag{2.6}$$

The traction has the same orientation as the force **F** and is a function of the unit normal vector $\hat{n}$. If we denote the vector $\hat{n} = \hat{e}_1, \hat{e}_2, \hat{e}_3$, then the traction vector **t** can be written as follows (Figure 2.2):

$$\underline{t}^{(\hat{e}_1)} = t_1^{\hat{e}_1}\hat{e}_1 + t_2^{\hat{e}_1}\hat{e}_2 + t_3^{\hat{e}_1}\hat{e}_3$$
$$\underline{t}^{(\hat{e}_2)} = t_1^{\hat{e}_2}\hat{e}_1 + t_2^{\hat{e}_2}\hat{e}_2 + t_3^{\hat{e}_2}\hat{e}_3$$

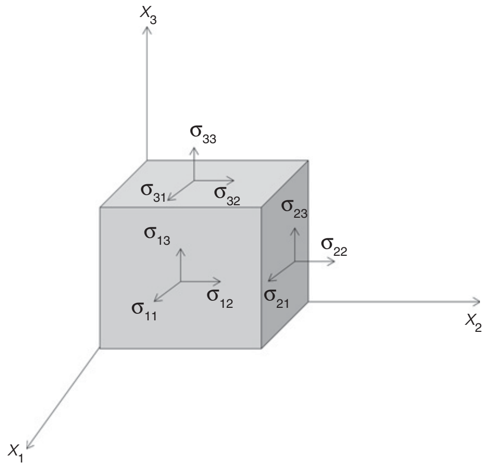

Figure 2.3 Stress components.

$$\underline{t}^{(\hat{e}_3)} = t_1^{\hat{e}_3}\hat{e}_1 + t_2^{\hat{e}_3}\hat{e}_2 + t_3^{\hat{e}_3}\hat{e}_3 \tag{2.7}$$

The stress tensor completely describes the surface forces acting on a body. We can describe the force on a surface oriented in a direction $\hat{n}$ as (Figure 2.1)

$$\underline{t} = \underline{\underline{\sigma}} \cdot \hat{n},\ or\ t_i = \sum_{j=1}^{3} \sigma_{ij} n_j = \sigma_{ij} n_j,\ [\sigma_{ij}] = \begin{bmatrix} \sigma_{11} & \sigma_{12} & \sigma_{13} \\ \sigma_{21} & \sigma_{22} & \sigma_{23} \\ \sigma_{31} & \sigma_{32} & \sigma_{33} \end{bmatrix} \tag{2.8}$$

We note that repeated indices imply summation. Note that stress is a tensor of second order. A tensor of second order dotted into a vector yields a vector (tensor of order 1). The dot product of tensors is equivalent to the reduction in the order of the tensor. In this case, the dot product of stress (second-rank tensor) with unit normal $\hat{n}$ (vector or first-rank tensor) will be a traction vector (first-rank tensor).

The diagonal elements of the stress matrices are defined as the normal stresses, and the off-diagonal element are the shear stresses.

Equilibrium

Equilibrium at an arbitrary volume V of the continuum, subjected to a set of surface tractions $\boldsymbol{t_i}$ and body forces $\boldsymbol{b_i}$ (including inertia forces, if present), is given by the integral relation

$$\int_S t_i^{\mathrm{n}}\, dS + \int_V \rho b_i\, dV = 0 \tag{2.9}$$

The divergence theorem of Gauss relates the volume integral to a surface integral so that $\int_S \underline{V} \cdot \hat{n} dS = \int_V \nabla \cdot \underline{V} dV$. This relation can be expanded to a tensor field T_{ijkl} of any rank such that $\int_S \underline{T} \cdot \hat{n} dS = \int_V \nabla \cdot \underline{T}\, dV$. Thus the equilibrium relation can be expressed as

$$\int_V (\sigma_{ji,j} + \rho b_i) dV = 0 \tag{2.10}$$

As this must be true for every volume V, the equilibrium relation can be stated as

$$\sigma_{ji,j} + \rho b_i = 0 \ or \ \nabla \cdot \underline{\underline{\sigma}} + \rho \underline{b} = 0 \tag{2.11}$$

Stress Tensor Symmetry

The stress tensor must be symmetric for a body to be in equilibrium and have no net rotation in it, i.e., $\sigma_{ij} = \sigma_{ji}$. Thus the number of independent stress components is six.

> ### Transformation of Vectors and Tensors
>
> Transformation of vectors from one coordinate system to another are given by equation (2.3). Transformation of stress from $[x_1, x_2, x_3]$ into a new coordinate system $[x_1', x_2', x_3']$ is given by $\underline{\underline{\sigma}}' = \underline{\underline{Q}}\ \underline{\underline{\sigma}}\ \underline{\underline{Q}}^T$ in equation (2.3) and proved in equation (2.12):
>
> $$\begin{gathered} \underline{T} = \underline{\underline{\sigma}}\hat{n} \\ \underline{T}' = Q\underline{T} = Q(\underline{\underline{\sigma}}\hat{n}) = Q\underline{\underline{\sigma}}Q^T Q\hat{n} \\ Q\hat{n} \equiv \hat{n}'; \ Q\underline{\underline{\sigma}}Q^T \equiv \underline{\underline{\sigma}}' \Rightarrow \underline{T}' = \underline{\underline{\sigma}}'\hat{n}'. \end{gathered} \tag{2.12}$$

Any symmetric tensor can be transformed into a coordinate system where the off-diagonal elements are zero. Thus, there is a coordinate system where the stress is given by a diagonal 3 × 3 matrix:

$$\underline{\underline{\sigma}}' = Q\underline{\underline{\sigma}}Q^T, \ [\underline{\underline{\sigma}}'_{ij}] = \begin{bmatrix} \sigma'_{11} & 0 & 0 \\ 0 & \sigma'_{22} & 0 \\ 0 & 0 & \sigma'_{33} \end{bmatrix} \tag{2.13}$$

This coordinate system is called the principal one, and $[x_1', x_2', x_3']$ are called the principal axes. The diagonal elements of the stresses in the principal axes are defined as principal stresses.

Principal Stresses

In a principal stress space (i.e., a space whose axes are in the principal stress directions) the traction is given by

$$\begin{bmatrix} \sigma_1 & & \\ & \sigma_2 & \\ & & \sigma_3 \end{bmatrix} \begin{bmatrix} n_1 \\ n_2 \\ n_3 \end{bmatrix} = \begin{bmatrix} t_1 \\ t_2 \\ t_3 \end{bmatrix} \tag{2.14}$$

or $\underline{t}^{(\hat{n})} = \underline{\underline{\sigma}}\hat{n}$

Maximum and Minimum Shear Stress

Consider the traction vector $\boldsymbol{t}$ resolved into the orthogonal normal and tangential components. The magnitude of the shearing or tangential component is given by

$$\sigma_S^2 = t_i^{(\hat{n})} t_i^{(\hat{n})} - \sigma_N^2 \tag{2.15}$$

The normal stress is given by

$$\sigma_N = (\boldsymbol{\sigma} \cdot \hat{n}) \cdot \hat{n} = \sigma_1 n_1^2 + \sigma_2 n_2^2 + \sigma_3 n_3^2 \tag{2.16}$$

Substituting equation (2.16) into (2.15), we get that the shear stress as a function of the direction cosines of the unit normal is given by

$$\sigma_S^2 = \sigma_1^2 n_1^2 + \sigma_2^2 n_2^2 + \sigma_3^2 n_3^2 - (\sigma_1 n_1^2 + \sigma_2 n_2^2 + \sigma_3 n_3^2)^2 \tag{2.17}$$

The maximum and minimum shear stress values may be obtained from equation (2.17) (Malvern, 1969). It can be shown that the minimum shear stress is zero in the principal coordinate system (i.e., where $\sigma_1, \sigma_2, \sigma_3$ are in the normal direction). The maximum shear stress occurs when the direction cosines are at ±45°.

Mohr's Circles for Stress

From equations (2.16) and (2.17) we get that

$$\begin{aligned} \sigma_N &= \sigma_1 n_1^2 + \sigma_2 n_2^2 + \sigma_3 n_3^2 \\ \sigma_N^2 + \sigma_S^2 &= \sigma_1^2 n_1^2 + \sigma_2^2 n_2^2 + \sigma_3^2 n_3^2 \end{aligned} \tag{2.18}$$

Combining equation (2.18) with the fact that $(n_1)^2 + (n_2)^2 + (n_3)^2 = 1$, we can solve for the direction cosines and get the following equations, which are the basis of Mohr's stress circles:

$$\begin{aligned} n_1^2 &= \frac{(\sigma_N - \sigma_2)(\sigma_N - \sigma_3) + \sigma_S^2}{(\sigma_1 - \sigma_2)(\sigma_1 - \sigma_3)} \\ n_2^2 &= \frac{(\sigma_N - \sigma_1)(\sigma_N - \sigma_3) + \sigma_S^2}{(\sigma_2 - \sigma_3)(\sigma_2 - \sigma_1)} \\ n_3^2 &= \frac{(\sigma_N - \sigma_2)(\sigma_N - \sigma_1) + \sigma_S^2}{(\sigma_3 - \sigma_1)(\sigma_3 - \sigma_2)} \end{aligned} \tag{2.19}$$

Mohr's stress circles are a convenient 2D graphical representation of the 3D stress tensor as demonstrated in Figure 2.4.

All stress points must be in the shaded region in Figure 2.4. This can be shown using geometrical reconstruction of directional cosines on a unit sphere (Malvern, 1969).

Mohr–Coulomb Failure Criteria

The Mohr–Coulomb failure criterion represents the linear envelope that is obtained from a plot of the shear strength of the material versus applied normal stress. The relation is written as

$$\sigma_c = c_0 + \sigma_N \tan\varphi \tag{2.20}$$

where c_0 is the cohesion and φ is known as the angle of internal friction.

In its basis, Mohr–Coulomb failure is nothing but a static internal friction law where shear failure occurs when the shear force on a plane reaches the failure line σ_c. Here c_0 is the cohesion, and it defines the strength of the rock (in terms of resistance to shear failure) when the normal stress is zero. For unconsolidated sediments and soils, $c_0 = 0$, which means that under no stress, there is no resistance to shear.

Figure 2.5 demonstrates the shear failure associated with equation (2.20). When the normal stress is negative, the failure mode is considered as tensile failure, which may not follow the same line defined in equation (2.20). Also, it is important to note that failure and deformation are complicated processes that will be discussed in more detail in the next sections.

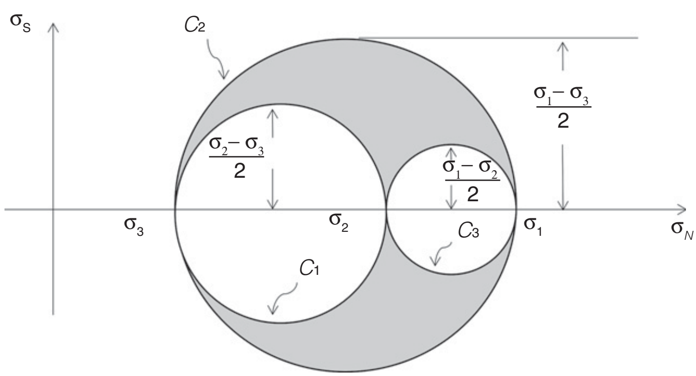

Figure 2.4 Mohr's stress circle.

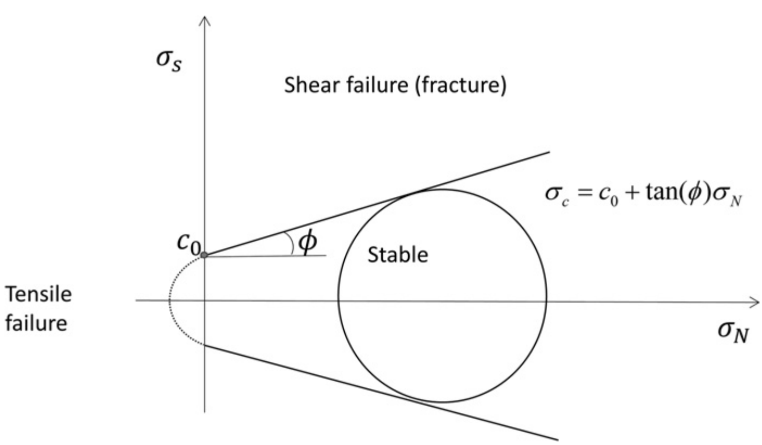

Figure 2.5 Mohr–Columb failure criteria are for stresses whose normal and shear components lie above the shear failure line.

Plane Stress

The state of stress when one principal stress is zero is known as plane stress. At this point the Mohr's stress circle will have one of the principal stresses aligned with the origin, and therefore they will plot as in Figure 2.6.

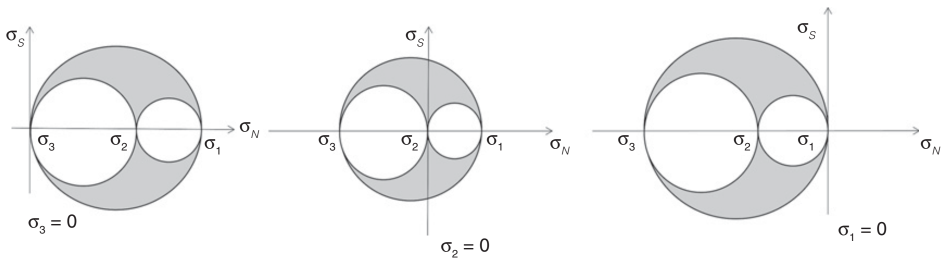

Figure 2.6 Mohr's circle and plane stress.

2.3 Deformation and Strain

In general we distinguish finite strain from infinitesimal strain. Large strains which are associated with large deformation processes in the earth such as failure and compaction often require us to use either large strain and, or discontinuity assumptions such as fractures and cracks. Small deformations are associated with the elastic region and specifically are appropriate when analyzing elastic wave propagation. When dealing with finite strain tensors, one needs to consider a Lagrangian or Eulerian description point of view and define the finite strain tensors between the undeformed and deformed configuration. In linear elasticity and especially elastodynamics it can be shown that the Eulerian and Lagrangian descriptions are equivalent (see Ben Menahem and Singh, 1980, for discussion). Further discussion on finite strain is not within the scope of this book; we refer the reader to a standard textbook on continuum mechanics for more information.

2.3.1 Infinitesimal Strains

When an elastic body is subjected to stresses, deformation results. The strain tensor describes the deformation resulting from differential motion within the body. Figure 2.7 shows the deformation possible to a body, with the initial (undeformed) and deformed Cartesian coordinate axes $[X_1, X_2, X_3]$ and $[x_1, x_2, x_3]$, respectively, sharing the same origin. The particles Q_0 and P_0 in the undeformed configuration move to Q and P in the deformed configuration. We can describe the first-order deformation by expanding the distortion of the body into a Taylor series:

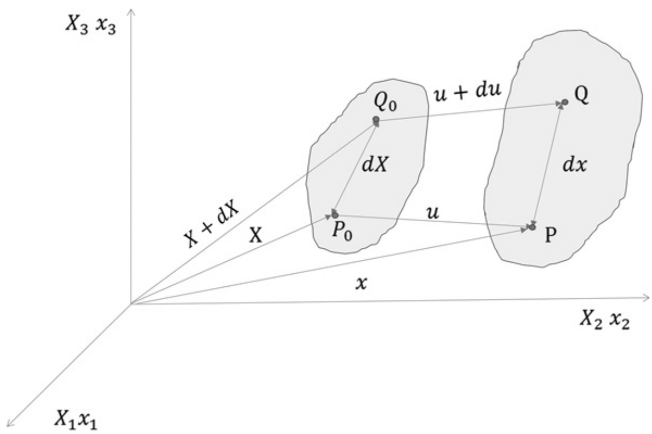

Figure 2.7 Deformation of a continuous body.

$$u_i(\underline{x} + \delta\underline{x}) \approx u_i(\underline{x}) + \frac{\partial u_i(\underline{x})}{\partial x_j}\delta\underline{x} = u_i(\underline{x}) + \delta u_i$$

$$\delta u_i = \frac{\partial u_i(\underline{x})}{\partial x_j}\delta\underline{x} \tag{2.21}$$

The relative displacement near $\underline{x}$ to the first order is δu_i.

Equation (2.21) involves the 3×3 matrix $\frac{\partial u_i(\underline{x})}{\partial x_j}$ that is dotted into the $\delta\underline{x}$ vector. The expression can be always decomposed into a symmetric and antisymmetric parts as follows:

$$\delta u_i = \frac{1}{2}\left[\frac{\partial u_i}{\partial x_j} + \frac{\partial u_j}{\partial x_i}\right]\delta x_j + \frac{1}{2}\left[\frac{\partial u_i}{\partial x_j} - \frac{\partial u_j}{\partial x_i}\right]\delta x_j = (e_{ij} + \omega_{ij})\delta x_j \tag{2.22}$$

where the ω_{ij} term corresponds to a rigid body rotation without deformation. The e_{ij} term is the strain tensor describing the internal deformation of the material. Its components in the $[x, y, z]$ system are:

$$[e_{ij}] = \begin{bmatrix} \frac{\partial u_x}{\partial x} & \frac{1}{2}\left[\frac{\partial u_x}{\partial y} + \frac{\partial u_y}{\partial x}\right] & \frac{1}{2}\left[\frac{\partial u_x}{\partial z} + \frac{\partial u_z}{\partial x}\right] \\ \frac{1}{2}\left[\frac{\partial u_y}{\partial x} + \frac{\partial u_x}{\partial y}\right] & \frac{\partial u_y}{\partial y} & \frac{1}{2}\left[\frac{\partial u_y}{\partial z} + \frac{\partial u_z}{\partial y}\right] \\ \frac{1}{2}\left[\frac{\partial u_z}{\partial x} + \frac{\partial u_x}{\partial z}\right] & \frac{1}{2}\left[\frac{\partial u_z}{\partial y} + \frac{\partial u_y}{\partial z}\right] & \frac{\partial u_z}{\partial z} \end{bmatrix} \tag{2.23}$$

The strain tensor can be expressed in a principal coordinate system as well (symmetric tensor). In this coordinate system the trace or sum of the eigenvalues (diagonal elements), is known as the *dilatation*, and it is equal to the divergence of the displacement field $u(x)$:

$$\theta = e_{ii} = \frac{\partial u_1}{\partial x_1} + \frac{\partial u_2}{\partial x_2} + \frac{\partial u_3}{\partial x_3} = \nabla \cdot \underline{u} \tag{2.24}$$

Volumetric strain: Dilatation

Dilatation represents to the first order the change in volume $V = dx_1 dx_2 dx_3$ associated with the deformation. This is shown in the derivation below:

$$\begin{aligned} V + \Delta V &= \left[1 + \frac{\partial u_1}{\partial x_1}\right] dx_1 \left[1 + \frac{\partial u_2}{\partial x_2}\right] dx_2 \left[1 + \frac{\partial u_3}{\partial x_3}\right] dx_3 \\ &\approx \left[1 + \frac{\partial u_1}{\partial x_1} + \frac{\partial u_2}{\partial x_2} + \frac{\partial u_3}{\partial x_3}\right] dx_1 dx_2 dx_3 \\ &= [1+\theta]V \;\Rightarrow\; V + \Delta V \approx [1+\theta]V,\;\; \theta = \frac{\Delta V}{V} \end{aligned} \tag{2.25}$$

Additional strain components of interest are the extensional strain, defined as the relative change in length of a material undergoing one dimensional extension.

$$\begin{aligned} &\Delta L = L - L_0 = u(x+dx) - u(x) \approx \frac{\partial u}{\partial x} L_0 \;\Rightarrow \\ &\frac{\Delta L}{L_0} \approx \frac{\partial u}{\partial x} \equiv e_{xx} \end{aligned} \tag{2.26}$$

Therefore the elements on the diagonal of the strain tensors are related to the deformation of the body along the principal directions. Figure 2.8 shows dilatation and extensional strains.

Shear Strain

The off-diagonal components of the strain tensor are interpreted as pure shear. This can be demonstrated as follows: Consider the deformation described in Figure 2.9 where a square body element is deformed by angle α Then $\tan\alpha = \frac{\partial u_x}{\partial y} = \frac{\partial u_y}{\partial x}$. For small angles we get $\tan\alpha \approx \alpha \approx \frac{1}{2}\left[\frac{\partial u_x}{\partial y} + \frac{\partial u_y}{\partial x}\right]$.

2.4 Fundamental Laws of Continuum Mechanics

We state here without proofs the fundamental laws of continuum mechanics. We refer the reader to continuum mechanics textbook (e.g., Malvern, 1969) for a complete discussion.

2.4.1 Conservation of Mass

Total mass in a volume will not change in time, in the absence of sources or sinks. This can be posed mathematically as

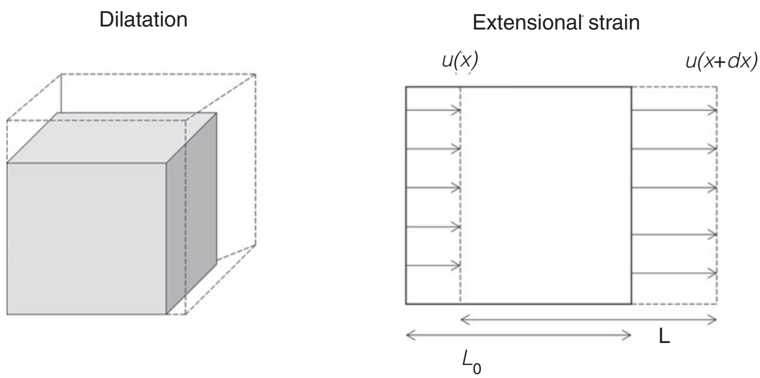

Figure 2.8 Dilation (left) is a volumetric deformation of a solid element. Extensional strain is the deformation of the element along one direction such that $du/dx \sim (L_0 - L)/L_0$.

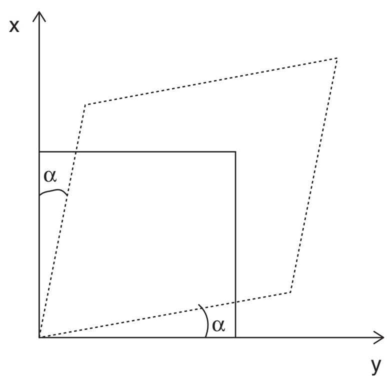

Figure 2.9 Shear strain: A square body element is deformed by angle α. Then $\tan \alpha = \frac{\partial u_x}{\partial y} = \frac{\partial u_y}{\partial x}$. For small angles we get $\tan \alpha \approx \alpha \approx \frac{1}{2}\left[\frac{\partial u_x}{\partial y} + \frac{\partial u_y}{\partial x}\right]$, which is the shear strain.

$$
\begin{aligned}
m &= \int_V \rho(\boldsymbol{x}, t) dV \\
\frac{dm}{dt} &= \frac{d}{dt}\int_V \rho(\boldsymbol{x}, t) dV = \int_V \left(\frac{d}{dt}\rho(\boldsymbol{x}, t) + \rho \nabla \cdot v\right) dV = 0
\end{aligned} \tag{2.27}
$$

where v is the velocity.

2.4.2 Equation of Motion

Change in momentum P is equal to the sum of body forces and surface tractions acting on the material

$$\begin{aligned} &\boldsymbol{P}=\int\limits_V \rho(\boldsymbol{x},t)\boldsymbol{v}dV \\ &\int\limits_S t^{(\hat{n})}dS+\int\limits_V \rho(\boldsymbol{x},t)\boldsymbol{b}dV=\frac{d\boldsymbol{P}}{dt}\leftrightarrow\int\limits_V\Big(\nabla\cdot\boldsymbol{\sigma}+\rho(\boldsymbol{x},t)\boldsymbol{b}\Big)dV=\frac{d\boldsymbol{P}}{dt} \end{aligned} \tag{2.28}$$

In equilibrium we get

$$\begin{aligned} &\int\limits_V\Big(\nabla\cdot\boldsymbol{\sigma}+\rho(\mathbf{x},t)\mathbf{b}\Big)dV=0 \\ &\nabla\cdot\boldsymbol{\sigma}+\rho(\mathbf{x},t)\mathbf{b}=0 \\ &or \\ &\sigma_{ij,j}+\rho b_i=0 \end{aligned} \tag{2.29}$$

where repeated indices imply summation.

2.4.3 Conservation of Angular Momentum

Change in angular momentum N is equal to the sum of surface integral over traction moments and volume integral over body force moment:

$$\begin{aligned} &\boldsymbol{N}=\int\limits_V(\boldsymbol{x}\times\rho\mathbf{v})dV \\ &\int\limits_S\Big(\boldsymbol{x}\times t^{(\hat{n})}\Big)dS+\int\limits_V\Big(\boldsymbol{x}\times\rho(\boldsymbol{x},t)\boldsymbol{b}\Big)dV=\frac{d\boldsymbol{N}}{dt} \end{aligned} \tag{2.30}$$

2.4.4 Conservation of Energy: First Law of Thermodynamics

The first law of thermodynamics relates the work done on the system and the heat transfer into the system to the change in energy of the system.

Considering K as the elastic energy in the material, U the potential energy, and total work done W, the first law of thermodynamics can be written as

$$\frac{dK}{dt}+\frac{dU}{dt}=\frac{d^*W}{dt}$$

The conservation of energy implies the following equilibrium:

$$\overbrace{\sigma:\dot{\varepsilon}}^{\text{strain energy}}+\overbrace{Q}^{\text{internal heat generation}}-\overbrace{\nabla\cdot q}^{\text{heat flux}}=\overbrace{\rho\frac{du}{dt}}^{\text{kinetic energy}} \tag{2.31}$$

The term d*W/dt denotes that it is not an exact differential.

2.4.5 Equation of State, Second Law of Thermodynamics

Entropy grows with irreversible process and the change in entropy is equal to zero in reversal processes. In loose terms, entropy defines a measure of disorder in a system and is often related to the fact that conversion between mechanical energy and heat increase is imperfect.

Define L as volumetric entropy and s as entropy density. Then

$$\begin{aligned} L &= \int_V \rho s dV \\ ds &= ds^{(e)} + ds^{(i)} \end{aligned} \tag{2.32}$$

where $ds^{(e)}, ds^{(i)}$ are increments in specific entropy due to interaction with exterior (e) and internal (i) increments. Then the second law of thermodynamics requires that

$$\begin{aligned} &ds^{(i)} > 0 \text{ (irreversible process)} \\ &ds^{(i)} = 0 \text{ (reversible process)} \end{aligned} \tag{2.33}$$

i.e., if we assign external entropy to a system, its total entropy will increase if the process is irreversible or, if the process is reversible, will be exactly equal to the external increment.

2.4.6 Clausius–Duhem Inequality, Dissipation Function

According to the second law of thermodynamics, the rate of entropy increase is greater than or equal to the entropy input rate. This is known as the Clausius–Duhem inequality. From statistical mechanics, there is an energy dissipation function associated with irreversible processes. In a continuum undergoing a reversible process such as a perfect spring undergoing deformation and expansion there will be no energy dissipation. For irreversible thermodynamics an energy dissipation function proportional to the entropy production rate can be defined. This function is positive definite. An example of using this concept will be presented in a later section when poroelasticity is discussed.

2.5 Hooke's Law and Constitutive Equations

The relation between the stresses applied to the material and the strains resulting from it is called a *constitutive equation*. Each material behaves differently, and there are many models to describe different materials.

One of the simplest types of materials is called *linearly elastic* material. For this material the relation between stress and strain can be expressed by a linear relation called *Hooke's law*:

$$\sigma_{ij} = C_{ijkl} e_{kl} \leftrightarrow \underline{\underline{\sigma}} = \underline{\underline{\underline{\underline{C}}}}\, \underline{\underline{e}} \tag{2.34}$$

The elastic constants C_{ijkl} are called the elastic moduli of the material. C_{ijkl} is a fourth-order tensor (relates a second-order tensor to a second-order tensor in the same way that a second-order tensor relates a first-order tensor (vector) to a first-order tensor).

A fourth-order tensor in a 3D system can have 3^4 independent variables. But the elastic tensor is symmetric ($C_{ijkl} = C_{jikl}$; $C_{ijkl} = C_{jilk}$), which makes the number of independent constants to be 36 (6 independent stress components and 6 independent strain components). Further reduction in the number of independent coefficients to 21 can be shown when considering the strain energy symmetry. The strain energy is defined as

$$u^* = \frac{1}{2}\sigma_{ij}e_{ij} = \frac{1}{2}C_{ijkl}e_{kl}e_{ij} \tag{2.35}$$

While in its most general form the elastic stiffness matrix consist of 21 constants, the simplest type of elastic material is the one that is *isotropic*. For isotropic media the elastic tensor C_{ijkl} can be expressed as

$$C_{ijkl} = \lambda\delta_{ij}\delta_{kl} + \mu(\delta_{ik}\delta_{jl} + \delta_{il}\delta_{jk})$$

where λ and μ are Lamé constants. The relation between stress and strain can be expressed as

$$\sigma_{ij} = \lambda e_{kk}\delta_{ij} + 2\mu e_{ij} = \lambda\theta\delta_{ij} + 2\mu e_{ij} \tag{2.36}$$

or

$$\begin{aligned} \sigma_{ij} &= \lambda\theta + 2\mu e_{ii}, \quad i = (x, y, z) \\ \sigma_{ij} &= 2\mu e_{ij}, \qquad\quad i = (x, y, z), i \neq j \end{aligned} \tag{2.37}$$

When material properties are directional, the material is said to be anisotropic. Lame's coefficient μ, is also known as the shear modulus. In engineering notation the shear modulus is often referred to as G. To facilitate communication between the geophysics and engineering terminology, we will refer in the following chapters to the shear modulus as G while Lame's parameter μ, will be used interchangeably, but will be referred to as Lame's parameter.

2.5.1 Elastic Constants for Isotropic Media

Although Lamé coefficients are very convenient we often use other elastic moduli or constants. The most common are *Young's modulus E*, *bulk modulus K*, and *Poisson's ratio v*. These represent specific tests.

Consider a medium in which all stresses are zero but σ_{xx}. Then for positive σ_{xx}, e_{xx} will increase and e_{yy} and e_{zz} will typically decrease. *Young's modulus* is defined as

$$E = \frac{\sigma_{xx}}{e_{xx}}. \tag{2.38}$$